VARIATION OF SUMMER PHYTOPLANKTON COMMUNITY COMPOSITION AND ITS RELATIONSHIP TO NITRATE AND REGENERATED NITROGEN ASSIMILATION ACROSS THE NORTH ATLANTIC OCEAN

N. Van Oostende[1], S. E. Fawcett[1,2], D. Marconi[1], J. Lueders-Dumont[1], A. J. M. Sabadel[3,4], E. M. S. Woodward[4], B. F. Jönsson[1], D. M. Sigman[1] and B. B. Ward[1]

[1] Department of Geosciences, Princeton University, Princeton New Jersey, USA
[2] Department of Oceanography, University of Cape Town, Cape Town, South Africa
[3] Department of Chemistry, University of Otago, Dunedin, New Zealand
[4] Plymouth Marine Laboratory, Plymouth, United Kingdom

contact email: oostende@Princeton.EDU

Abstract

The North Atlantic Ocean is considered a nitrogen (N) limited system once vernal stabilisation of the water column alleviates light limitation and allows phytoplankton growth to deplete surface nutrients to virtually undetectable levels. Ammonium and other regenerated N forms are then the main surface N source for phytoplankton production. The effort to determine which phytoplankton groups contribute to long-term biological export production would be greatly aided by information on which phytoplankton groups are responsible for the assimilation of nitrate, as opposed to those assimilating predominantly regenerated N. In this study, we used the natural abundance N isotopes to examine basin-scale patterns of nitrate and regenerated N assimilation and evaluated the relationships between these trends and phytoplankton community composition. Samples were collected during a summertime cruise transect (August-September 2013) from the subtropical (36°N 73°W) to the subarctic (54°N 20°W) North Atlantic and analysed for the N isotopic composition ($\delta^{15}N$ vs. N_2 in air) of particulate nitrogen (PN) and nitrate, size-fractionated chlorophyll *a*, and phytoplankton group biomass using flow cytometry. The depth of the 300 nmol l^{-1} nitrate isopleth shoaled from the subtropics (79 m), where phytoplankton stripped surface waters of nitrate, to the subarctic, where it intersected with the surface and the upward nutrient supply drove a summer phytoplankton bloom. The $\delta^{15}N$ of PN above the nitracline increased from the subtropics (-0.3‰) to the subarctic (4.2‰), reflecting both a change in the $\delta^{15}N$ of the subsurface nitrate source (from 2.4‰ to 5.1‰) and increased reliance by phytoplankton on nitrate relative to regenerated N. Throughout the transect, the phytoplankton community was mainly composed of pico- and nano-sized cells (>88% of chlorophyll *a* in the <20 µm size fraction). In the part of the transect southwest of the Grand Banks, *Prochlorococcus* and *Synechococcus* together dominated the picophytoplankton biomass (58% and 18% on average) and comprised 35% and 9%, respectively, of combined pico- and nanophytoplankton biomass. Pico- and nanoeukaryotes showed the opposite pattern, becoming more

important closer to the subarctic (up to 31% and 86% of combined pico- and nanophytoplankton biomass, respectively). The North Atlantic summertime patterns in N assimilation implied by the N isotopes were consistent with a higher degree of nitrate assimilation by larger eukaryotic cells and greater reliance on regenerated N by cyanobacterial picophytoplankton, congruent with the observed biomass distributions.

Keywords:

nitrate utilization, nitrogen assimilation, nitrogen isotopes, phytoplankton community composition, flow cytometry, North Atlantic Ocean

1. Introduction

According to the classical paradigm, the amount of new production, which drives the biological pump, is controlled by light intensity, the supply rate of nitrate and other nutrients (phosphorus, iron) to the euphotic zone, and the degree to which these nutrients are consumed by phytoplankton (Dugdale and Goering, 1967). In contrast, regenerated production is supported by forms of nitrogen (N) recycled in the euphotic zone (predominantly ammonium and urea (Saito *et al.*, 2014), and potentially augmented by *in situ* ammonia and nitrite oxidation) and, from a mass balance perspective, does not contribute to long-term export production (Eppley and Peterson, 1979). Dinitrogen (N_2) fixation, atmospheric deposition and riverine input also contribute reactive N species that fuel new production, but their annual flux to the surface ocean is minor compared to that of subsurface nitrate in the North Atlantic Ocean (Altieri *et al.*, 2016; Deutsch *et al.*, 2007; Duce *et al.*, 2008; Gruber and Sarmiento, 1997; Oschlies, 2002). Understanding the mechanisms responsible for the patterns of primary production and nutrient cycling in the ocean in part requires improved knowledge of the spatial distribution of biodiversity and its associated biogeochemical activities.

Phytoplankton have adapted to thrive in the range of nutrient regimes -from oligotrophic to mesotrophic- and light regimes -from stable low- or high-light conditions to highly variable conditions– that occur in the ocean. Seasonal changes in insolation and heat flux, major hydrographic features such as ocean currents and fronts, as well as shorter-lived mesoscale eddies and meteorological events all structure the distribution of phytoplankton assemblages and shape their nutrient uptake potential across the oceans (d'Ovidio *et al.*, 2010; Garçon *et al.*, 2001; Sambrotto *et al.*, 1993). In turn, the species composition and cell size structure of the plankton assemblage are often characteristic of their immediate environment and its physicochemical history.

The North Atlantic Ocean is classically considered an N-limited system (Moore *et al.*, 2013), becoming N and P co-limited further south (e.g. Moore *et al.* (2008)) and N and Fe co-limited further north (e.g. Nielsdóttir *et al.* (2009)), once the water column stratifies in spring and summer and phytoplankton are released from the light limitation of winter. The North Atlantic spring bloom constitutes one of the largest biological signals on Earth and is characterised by a succession of phytoplankton groups (Lochte *et al.*, 1993; Sieracki *et al.*, 1993). The decreasingly turbulent, nutrient-rich, springtime conditions are characterised by fast-growing diatom-dominated planktonic communities associated with high rates of new production and export production until silicate is exhausted (Alkire *et al.*, 2014; Cetinić *et al.*, 2015; Rynearson *et al.*, 2013). These high-biomass diatom blooms are then succeeded by communities of smaller phytoplankton species (e.g., coccolithphores) and mixotrophic flagellate species (e.g., dinoflagellates) in the more quiescent and nutrient-deplete summertime conditions, or in water masses originating from the subtropics (Barton *et al.*, 2013; Dandonneau *et al.*, 2004; Tarran *et al.*, 2001).

At lower chlorophyll *a* concentrations ([Chla]<1 mg m^{-3}), which are typically observed in low nutrient supply systems, the smallest nano- and picophytoplankton size-fractions make up the largest share of total Chla (Chisholm, 1992; Marañón *et al.*, 2012; Raimbault *et al.*, 1988). The dominance of the pico- and nanophytoplankton biomass in this case is reflected in their substantial contribution

to primary productivity (Joint *et al.*, 1993; Marañon *et al.*, 2001). Beyond the partitioning of phytoplankton functional groups into size classes (Sieburth *et al.*, 1978), techniques such as flow cytometry have allowed quantification of at least some of their considerable phylogenetic and functional diversity (e.g., the distinction between phycoerythrin-containing cyanobacteria and coccolithophores), therefore allowing for extensive sampling and recognition of macro-ecological patterns in phytoplankton community structure (Li, 1997, 2002; Tarran *et al.*, 2006). The picophytoplankton community (cell diameter <~2-3 μm), of which the prokaryotic cyanobacterial genera *Prochlorococcus* and *Synechococcus* are usually numerically dominant, also harbours a considerable amount of eukaryotic diversity (Hooks *et al.*, 1988; Kirkham *et al.*, 2013; Vaulot *et al.*, 2008). The larger cell size of these eukaryotes means that, although they are typically less numerically-abundant than the very small picocyanobacteria (cell diameter ~0.6-1.2 um), they often dominate the phytoplankton biomass (Li, 1995). The relatively larger nanophytoplankton, on the other hand, have only fairly recently been routinely measured using flow cytometry instead of epifluorescence microscopy or concentrations of marker pigments (Tarran *et al.*, 2006), which has allowed for higher sample throughput. The combination of phytoplankton community analysis with estimates of phytoplankton group biomass based on flow cytometric size measurements allows for a more quantitative understanding of the functioning of microbial communities (Laney and Sosik, 2014; Olson *et al.*, 1989; Rodríguez *et al.*, 1998; Zubkov *et al.*, 1998).

Intense biological activity during the spring and early summer in the North Atlantic depletes the surface nutrients (Joint *et al.*, 1993), and nutrient resupply from deeper waters is hampered by further strengthening of the pycnocline. This leads to microbial communities becoming increasingly dependent on regenerated forms of N for growth, such that they contribute less to new-, and by extension export-, production (Azam *et al.*, 1983; Eppley and Peterson, 1979; Pomeroy, 1974). However, some phytoplankton groups appear to be effective at assimilating nitrate at the low concentrations available at the base of the euphotic zone in oligotrophic systems, and/or contribute disproportionally to carbon export. For example,

pigment data from the subtropical North Atlantic suggest that nanoeukaryotes contribute equally to particulate organic carbon (POC) export and autotrophic biomass, while cyanobacteria contributions to POC export are one-tenth of their contribution to autotrophic biomass (Lomas and Moran, 2011). Moreover, recent observations from the western and eastern subtropical North Atlantic have shown the importance of picoeukaryotes in nitrate assimilation and their potential for export production compared to prokaryotic phytoplankton (Fawcett *et al.*, 2011; Painter *et al.*, 2014), even when euphotic zone nitrate concentrations are below the limit of conventional colorimetric detection techniques. These findings emphasise the need for investigation of the distribution and abundance of the diverse picoeukaryotic phytoplankton from oligo- to mesotrophic oceanic regimes.

Phytoplankton growth and community structure are closely linked to the availability and biogeochemistry of N. Natural variations in the N isotopes of nitrate and suspended particulate N (PN) provide an integrative view of the N cycling activity of upper ocean biota. Regional and local differences in the supply of N to the euphotic zone as either subsurface nitrate or recycled N will be reflected in the $\delta^{15}N$ of PN ($\delta^{15}N$, in per mille (‰) vs. N_2 in air, = $\{[(^{15}N/^{14}N)_{sample}/(^{15}N/^{14}N)_{air}] - 1\} \times 1000$). Under nitrate-deplete summertime conditions, N forms regenerated by euphotic zone biota (predominantly ammonium) are thought to support most phytoplankton growth (Dugdale and Goering, 1967; Eppley and Peterson, 1979). The $\delta^{15}N$ of ammonium produced by surface ocean recycling is inferred to be low based on the amplitude of the isotopic fractionation associated with its production (Checkley and Miller, 1989; Macko *et al.*, 1986; Silfer *et al.*, 1992). In addition to assimilation by phytoplankton, another possible fate for euphotic zone ammonium is oxidation to nitrite and then nitrate (i.e., nitrification), which has the potential to complicate estimates of new production (Yool *et al.*, 2007). However, like recycled ammonium, nitrate regenerated in euphotic zone waters will be low in $\delta^{15}N$ (DiFiore *et al.*, 2009; Fawcett *et al.*, 2011). This is because the combined isotope effect of ammonia and nitrite oxidation is significantly greater than that of ammonium and nitrite assimilation (14-19‰ vs. 0-3‰; Casciotti, 2009; Casciotti *et al.*, 2003; Hoch

168 *et al.*, 1992; Liu *et al.*, 2013; Mariotti *et al.*, 1981; Pennock *et al.*, 1996), resulting in
169 low-δ^{15}N N being preferentially channelled into the nitrate pool (Suppl. Text 2.1).
170 Thus, the assimilation of recycled N, be it ammonium or regenerated nitrate, will
171 produce euphotic zone PN that is low in δ^{15}N.

172 The δ^{15}N of subsurface ocean nitrate ranges between 2.4‰ and 5.1‰ in our
173 study region (see below; Marconi *et al.*, 2015). In the case of a high degree of
174 consumption of the gross nitrate supply and lacking substantial assimilation of
175 other (e.g., regenerated) N sources, the δ^{15}N of surface PN should approximate the
176 δ^{15}N of this source nitrate (Altabet and Francois, 1994). Thus, suspended PN
177 comprising mainly nitrate-assimilating phytoplankton will have a higher δ^{15}N than if
178 the main phytoplankton N source had been regenerated N (Altabet, 1988; Fawcett *et*
179 *al.*, 2011). Concomitant measurements of the δ^{15}N of PN and nitrate can therefore
180 offer a spatiotemporally integrated view of upper ocean N consumption and provide
181 more information about N transformation processes than measurements of N
182 concentrations alone.

183 The goal of this study was to determine the basin-scale patterns of N
184 assimilation across the North Atlantic Ocean and its relationship to the
185 phytoplankton community size-structure and composition. To this end, we assessed
186 primary production and N cycling using a suite of physical, ecological,
187 biogeochemical and isotopic measurements made along a summer transect from the
188 subtropical to the subarctic North Atlantic Ocean (Figure 1). We hypothesised that
189 the relative dominance of the phytoplankton community by pico- and
190 nanoeukaryotes, compared to cyanobacterial picophytoplankton, would increase
191 towards the subarctic North Atlantic in parallel with an increase in nitrate
192 assimilation as recorded by the δ^{15}N of upper ocean nitrate and PN.

193 ## 2. Methods and Materials

194

195 The cruise transect was carried out in late summer of 2013 (23rd of August
196 to 3rd of September) on board the *R/V Endeavor*, which sailed from Morehead City,

North Carolina (34.7°N 76.7°W) to the subarctic North Atlantic (54.0°N 20.4°W) (Figure 1). Daily conductivity-temperature-density (CTD) casts to 1000 m depth were performed at dawn, at 12 stations, at intervals of approximately 220 nautical miles (~410 km; table 1). At each station, water for the determination of chemical and biological variables was collected from 9 depths using a set of 12 Niskin bottles (30 l capacity). Surface water samples (5 m depth) were collected via the ship's clean seawater inflow at each station, and every 6 hours along the transect. Results from chemical, biological, and CTD measurements are available at BCO-DMO: http://www.bco-dmo.org/project/544343.

2.1. Hydrographic parameters

The depth of the mixed layer (MLD) was derived using a difference in density threshold of 0.045 kg m^{-3} from the water density value at 10 m depth (cf. de Boyer Montégut *et al.* (2004)). Because most CTD casts were performed at dawn, the euphotic zone depth (Z_{eu}), which we define as the depth at which light intensity is 1% of its surface value, was derived from each vertical chlorophyll *a* (Chla) profile (see below) by progressively integrating the water column Chla content [ΣChla] to simultaneously obtain [ΣChla] and Z_{eu} through an iterative process (described by Morel and Berthon (1989) and re-parameterised in Morel and Maritorena (2001)). Based on the work of Marra *et al.* (2014) in the western North Atlantic, and according to equation 3 in Boss and Behrenfeld (2010),

$$Z_{Ic} = log_{10}(0.17/0.98 \times PAR) \times (Z_{eu}/log_{10}(0.01)),$$

we assumed 0.17 moles quanta m^{-2} day^{-1} to be the compensation irradiance (Ic) below which light is insufficient to support net photoautotrophy. Although this Ic value may be an underestimate (Laws *et al.*, 2014), it encompassed the depth of maximum Chla concentration at the southwestern stations of our transect and did not significantly affect the [ΣChla] at the northeastern stations compared to higher Ic values found in the literature (cf. Letelier *et al.* (2004)). This light compensation depth (Z_{Ic}), the lower boundary of a stratum of constant daily integrated photon flux, was calculated using the previously-estimated Z_{eu} and the surface daily integrated photosynthetically available radiation (PAR) values obtained from NASA

227 Aqua Modis level 3 data. Because of the small light attenuation coefficient derived at
228 station 7, the bottom depth was used instead of Z_{eu} and Z_{lc}.

229 **2.2. Nutrient and chlorophyll measurements**

230 Seawater for nutrient assays was collected from the Niskin bottles attached
231 to the CTD/Rosette system into acid cleaned (10% HCl), 'aged' by multiple water
232 rinsing and soaking cycles, 60 ml HDPE (Nalgene) sample bottles. In most cases,
233 samples were analysed immediately for nutrients, and always within 2-3 hours of
234 collection. The micromolar nutrient analysis was carried out using a Bran and
235 Luebbe 5-channel (nitrate, nitrite, phosphate, silicate, ammonium) AAIII segmented
236 flow, colorimetric, autoanalyser, using classical proven analytical techniques
237 (Woodward and Rees, 2001). Micromolar detection limits for nitrate, nitrite, and
238 phosphate were 0.2 μmol l^{-1}, and for ammonium was 0.5 μmol l^{-1}. The concentration
239 of silicate was always within the detection limit of the analyser. The accuracy of the
240 measurements was 1-2%.

241 Nanomolar ammonium was analysed using a method based on the gas
242 diffusion of ammonia across a Teflon membrane driven by a differential *p*H
243 gradient, and detection by a Jasco fluorometer (adaptation of Jones (1991))
244 following its reaction with a fluorescent reagent. Nanomolar nitrate, nitrite, and
245 phosphate were detected using colorimetric methodologies as with the standard
246 segmented flow analyser, but using 2 m long Liquid waveguides capillary cells as the
247 analytical flow cells; the detection limits for nanomolar nitrate and phosphate were
248 1 nmol l^{-1}, and for nitrite was 0.5 nmol l^{-1}. The nitracline was defined as the
249 sampling depth in the upper 150 m of the water column at which the nitrate
250 concentration gradient was the steepest. The depth of the 300 nmol nitrate l^{-1}
251 isopleth was obtained from individual nutrient profiles through linear interpolation.

252 Clean handling techniques were employed to avoid any contamination of the
253 samples, particularly for the ammonium samples. Dura-Touch gloves were used at
254 all times and samples were not decanted or transferred, but were kept tightly closed
255 until just before ammonium analysis in order to avoid any contamination from
256 external sources. No water column nutrient samples were frozen or stored. All

sampling and handling techniques, whenever possible, followed the international nutrient GO-SHIP manual (Hydes *et al.*, 2010).

Discrete Chla samples were measured fluorometrically (Holm-Hansen and Riemann, 1978) at 6 depths spanning the surface, the bottom of the euphotic zone, and the mixed layer and Chla maximum depths. Up to 4 l of seawater, retrieved directly from the Niskin bottles or the surface seawater inflow, were sequentially filtered through a 20 µm pore-size polycarbonate filter, a 2 µm pore-size polycarbonate filter, and a 0.3 µm pore-size glass fiber filter (GF-75; Sterlitech; 47 mm diameter). Filtrations were performed in the dark under low vacuum (<200 mbar). The Chla filters were packaged into aluminium foil (GF filter) or a 5 ml cryovial (polycarbonate filters) and immediately frozen at -80 °C until analysis. Chlorophyll was extracted in 90% acetone at 4°C overnight and measured using a Turner Trilogy fluorometer, calibrated against a pure Chla standard (*Anacystis nidulans* Chla, Sigma-Aldrich, Saint-Louis, USA). Measurements were corrected for the fluorescence of phaeopigments after acidification with HCl (24 mM final concentration). Depth-integrated Chla was calculated using the fluorometric measurements from the CTD casts (Fluo), which were rescaled according to the relationship between $\log_{10}$[Chla] and $\log_{10}$[Fluo] (log_{10}[Chla] (ng l^{-1}) = 0.74 × log_{10}[Fluo] + 2.52; r^2=0.74, p<0.001, df=95) and checked for the absence of systematic residual errors. The proportion of Chla in each biomass size fraction along the depth profile was linearly interpolated using the point measurements of size-fractionated Chla. Depth-integrated Chla in each size fraction was calculated by trapezoidally integrating the rescaled [Fluo] over the water column to Z_{lc} or the MLD, whichever was deepest.

2.3. Nitrogen isotope measurements

Water column nitrate+nitrite: Seawater samples for analysis of the N isotopic composition of nitrate+nitrite and nitrate-only were collected unfiltered at regular depth intervals from the surface to 1000 m in 60 ml (>150 m) or 125 ml (<150 m) square-bottomed, wide-mouth HDPE bottles (Nalgene). Bottles were acid-washed and rinsed with deionised water prior to sampling. At sea, pre-labelled bottles and

287 caps were rinsed three times with sample water, filled to ~85% of the bottle
288 volume, and frozen upright at -20°C until analysis.

289 Isotopic analyses were conducted using the "denitrifier method", wherein
290 denitrifying bacteria lacking nitrous oxide (N_2O) reductase quantitatively convert
291 nitrate and nitrite in the sample to N_2O gas (Casciotti *et al.*, 2002; Sigman *et al.*,
292 2001) (see also Weigand *et al.* (2016)) for the updated protocol used for analysing
293 these samples). The isotopic composition of N_2O was then measured by gas
294 chromatography-isotope ratio mass spectrometry (GC-IRMS) using a purpose-built
295 on-line N_2O extraction and purification system and a Thermo MAT 253 mass
296 spectrometer. Seawater solutions of the international nitrate reference materials,
297 IAEA-N3 and USGS-34, as well as an in-house N_2O standard, were run in parallel
298 with the samples in order to monitor the quality of bacterial N conversion and mass
299 spectrometric measurements. The reference materials bracketed each group of ~10
300 samples and were used to correct the measured $\delta^{15}N$ to N_2 in air (Casciotti *et al.*,
301 2002; McIlvin and Casciotti, 2011; Sigman *et al.*, 2001). Data are reported here only
302 for samples with nitrate+nitrite concentrations ≥300 nmol l^{-1}.

303 The presence of nitrite, even at very low concentrations, can significantly
304 alter the isotopic composition of nitrate+nitrite relative to that of nitrate alone
305 (Fawcett *et al.*, 2015; Granger and Sigman, 2009; Marconi *et al.*, 2015; Smart *et al.*,
306 2015). In this study, we used the $\delta^{15}N$ of nitrate-only to avoid interference from the
307 isotopic composition of nitrite, which originates from the first step of nitrification or
308 is excreted by phytoplankton following intracellular nitrate reduction to nitrite
309 (Lomas and Lipschultz, 2006); it thus does not contribute to new production *sensu*
310 *strictu*. The mean difference between the $\delta^{15}N$ of nitrate+nitrite and the $\delta^{15}N$ of
311 nitrate-only in the upper 150 m was ~1‰, and this was mostly dependent on the
312 relative contribution of nitrite to the combined nitrate+nitrite pool (6% on average).
313 However, the nitrite concentration was significant at times, and the greatest $\delta^{15}N$
314 difference (~4.8‰) was observed where the contribution of nitrite to the
315 nitrate+nitrite pool was highest (32% at ~60°W; station 5 at 60 m).

316 In order to measure the $\delta^{15}N$ of nitrate-only for samples with a detectable
317 concentration of nitrite, a nitrite removal pre-treatment is required. The detection
318 limit for nitrite in this case was 2 nmol kg^{-1}. Samples collected between the surface
319 and ~125 m were treated for nitrite removal via the addition of 10 µl of sulphamic
320 acid solution per ml of sample, which converts sample nitrite to N_2 gas with a
321 reaction time of 2-8 minutes, followed by the addition of 5.5 µl of 2*M* NaOH per ml of
322 sample to restore the *p*H of the sample to ~7-9 (Granger and Sigman, 2009). The
323 pooled standard error for $\delta^{15}N$ was 0.04‰ and 0.11‰ (n ≥3) for nitrate+nitrite
324 and nitrate concentrations ≥0.5 µmol l^{-1} and <0.5 µmol l^{-1}, respectively. Hereafter,
325 "nitrate" in the text refers to nitrate-only, after the subtraction (for concentration)
326 or removal (for $\delta^{15}N$) of nitrite.
327 *Suspended particulate N:* Suspended PN was collected at various depths
328 throughout the euphotic zone, including within the surface mixed layer and at the
329 depth of maximum Chla concentration, by gentle vacuum filtration (<135 mbar), of
330 8 l of seawater through a GF-75 filter. Filters were transferred to pre-combusted
331 (500°C for 5 h) aluminium foil envelopes, and immediately frozen at -80°C until
332 analysis.
333 In the laboratory, the PN filters were dried in a desiccating oven at 40°C.
334 Three subsamples were cored from each filter and transferred to combusted 4 mL
335 glass Wheaton vials. PN was oxidised to nitrate using the persulphate oxidation
336 method of Knapp et al. (2005), and as modified by Fawcett et al. (2011; 2014); this
337 was conducted in a laminar flow hood equipped with an ammonia/amine filter.
338 Briefly, 2 ml of persulphate oxidising reagent (POR) were added to each sample vial,
339 as well as to triplicate vials containing a filter blank plus varying quantities of two L-
340 glutamic acid isotope standards, USGS-40 and USGS-41 (Qi *et al.*, 2003); this allows
341 determination of the N content and $\delta^{15}N$ of the POR+filter blank. The POR was made
342 by dissolving 2.5 g of 4× recrystallised, methanol-rinsed potassium persulphate and
343 2.5 g of sodium hydroxide in 100 ml of ultra high-purity deionised water. Following
344 POR addition, vials were autoclaved at 121°C for 55 minutes on a slow-vent setting,
345 after which sample *p*H was lowered to 6-8 using 12N HCl. The concentration and

346 δ^{15}N of the resultant nitrate was measured via chemiluminescent analysis (Braman
347 and Hendrix, 1989) and the denitrifier method (see above) (Casciotti *et al.*, 2002;
348 Sigman *et al.*, 2001). The final N content and δ^{15}N of the oxidised samples was
349 corrected for the POR+filter blank. N content was converted to PN concentration by
350 normalising to whole-filter area and volume of seawater filtered. For each station,
351 upper ocean average δ^{15}N-PN was calculated by trapezoidally integrating the PN
352 concentration from the surface to the nitracline depth or the MLD, whichever was
353 deepest, and then weighting the individual measurements of δ^{15}N-PN by the depth-
354 integrated PN concentration for each depth interval. In order to compare upper
355 ocean δ^{15}N-PN across the transect without the confounding effect of the variable
356 source nitrate δ^{15}N, the measured δ^{15}N of nitrate at 250 m or 300 m at each station
357 was subtracted from the mass-weighted average δ^{15}N-PN. Station 7 (bottom depth
358 of 57 m) was excluded from these calculations due to the uncertainty of the δ^{15}N of
359 its nitrate source and the potential impact of sedimentary processes on δ^{15}N-PN.

360 **2.4. Plankton abundance and biomass determination**

361 The cell abundance of pico- and nanophytoplankton (<~14 μm cell diameter)
362 was determined by flow cytometric analysis of 1500 μl of glutaraldehyde-preserved
363 (1% v/v) (Marie *et al.*, 1997) samples using a BD Accuri C6 flow cytometer equipped
364 with a blue laser (488 nm), at a flow rate of 100 μl min^{-1}, and a core diameter of 22
365 μm. Standard fluorescent bead solutions were prepared daily and used as an
366 internal standard to assess instrument performance, to standardise scatter and
367 fluorescence measurements (Rainbow Calibration Particles (8 peaks), BD
368 Biosciences), and to validate the flow rate (TruCount, BD Biosciences) for
369 quantitative applications. Each sample was run with fluorescent beads (YG beads,
370 0.94 μm Fluoresbrite® Yellow Green Microspheres, Polysciences, Inc.) as an internal
371 standard for forward scatter measurements.

372 Several phytoplankton groups were distinguished based on their forward
373 (FSC) and side scatter (SSC), Chla, and phycoerythrin (PE) fluorescence signals
374 (Table 2): the picophytoplankton (<~2.5 μm) group comprised PE-containing
375 *Synechococcu*s and non-PE-containing picoeukaryotes (picoEuks), the

nanophytoplankton groups (nanoEuks, >~2.5 - 14 μm) included PE-containing nanophytoplankton (PE-nanoEuk), non-PE-containing phytoplankton (noPE-nanoEuk), and coccolithophores (Cocco) (the latter group was identified based on their enhanced side scatter signal). Representative flow cytometry density plots from which the phytoplankton populations were identified are shown in Figure S1.

The picoplanktonic *Prochlorococcus* cells were counted in SYBR Green I-stained samples (Marie *et al.*, 1997), according to (Heywood *et al.*, 2006), because of the difficulty of discriminating unstained cells from background noise. The concentration of heterotrophic bacterial cells was determined by flow cytometric analysis of 250 μl of glutaraldehyde-preserved (1% v/v) and SYBR Green I-stained (1:7500) samples according to Marie *et al.* (1997) and Gasol and Del Giorgio (2000). The *Prochlorococcus* and heterotrophic bacteria samples were analyzed using a BD Accuri C6 flow cytometer, at a flow rate of 35 μl min^{-1}, and a core diameter of 16 μm. All plankton groups were gated and their abundance quantified using FlowJo software (Tree Star, Inc., www.flowjo.com).

The biovolume of phytoplankton cells analysed by flow cytometry was derived from forward scatter measurements of individual cells based on the polynomial relationship between the $\log_{10}$ of measured biovolumes of pico- and nanophytoplankton cells and the $\log_{10}$ of the peak area of their forward scatter signal (FSC-A) (Laney and Sosik, 2014). A calibration procedure, using bead stocks and an unidentified cultured picoeukaryote from the Sosik Lab at Woods Hole Oceanographic Institution, confirmed the inter-lab agreement of flow cytometry-derived biovolume estimates (Figure S2). Since the largest phytoplankton cell in the empirical relationship of Laney & Sosik (2014) had a cell diameter of 14 μm and the number of cells larger than this in our samples was negligable, only cells up to ~14 μm in diameter were included in the cell abundance and biovolume calculations. Cellular biomass was estimated according to the relationship between cellular biovolume (μm^3 $cell^{-1}$) and carbon content (pmol $cell^{-1}$) for glutaraldehyde preserved pico- and nanophytoplankton cells from (Verity *et al.*, 1992): $C = (0.433 / 12) \times biovolume^{0.863}$.

Although *Synechococcus* cells could readily be counted based on their size and their characteristic PE fluorescence, the high signal-to-noise ratio in the FSC-A channel of the Accuri precluded a reliable cell size estimate for particles smaller than 1 µm. Therefore, the biomass of *Synechococcus* was estimated using a conversion factor of 140 fg C $cell^{-1}$ assuming a cell diameter of 1 µm and 270 fg C μm^{-3} (Bertilsson *et al.*, 2003). The biomass of *Prochlorococcus* cells was calculated by using an average cellular carbon content of 53.5 fg C $cell^{-1}$ (Bertilsson *et al.*, 2003), which is very similar to the range of cellular carbon content determined by Casey *et al.* (2013) for *Prochlorococcus* in the euphotic zone.

2.5. Primary productivity

Primary production rates were determined with the ^{13}C-uptake technique using on-deck, running surface seawater-cooled incubations, which simulated the *in situ* irradiance conditions at three depths corresponding to 55%, 33%, and 1% of surface PAR. The incubations were started at dawn by adding 1.40 ml of a freshly prepared ^{13}C-labelled (99%) bicarbonate solution (for a final concentration of 200 µmol ^{13}C l^{-1}) to each light-shielded, mesh-wrapped polycarbonate incubation bottle, and lasted for 6.5 ± 0.2 h. The entire content (2300 ml) of each incubation bottle was then filtered through a combusted (450°C for 5 hours) GF-75 filter and frozen at -80°C until analysis on land. In the laboratory, frozen GF-75 filters were thawed and fumed with concentrated HCl for 6 h to remove inorganic carbon, after which they were dried in a desiccating oven at 60°C for at least 24 h. The rim and two sections of each filter were cut out, placed in tin capsules, pelletised, and analysed on a Europa Scientific 20/20 triple collector mass spectrometer. Measurements of particulate organic carbon (POC) mass and isotopic composition were corrected for the blank, which consisted of a tin capsule and a blank pre-combusted GF-75 section. Daily standard curves bracketing anticipated sample masses were run prior to samples, with urea as a laboratory standard, and the measured isotopic composition was calibrated using peach leaf (NIST-1547) and L-glutamic acid (USGS-40; (Qi *et al.*, 2003)) standards. Using the daily standard curves, the mass of POC in each sample was calculated. The hourly rate of photosynthetic carbon

fixation by the phytoplankton community was determined from duplicate incubation samples by normalising the rate of dissolved inorganic carbon (DIC) incorporation into POC to the length of the incubation, calculated following (Legendre and Gosselin, 1997). These hourly rates of photosynthetic carbon fixation were then adjusted to account for the deviation of surface seawater incubation temperature from *in situ* temperature using a Q_{10} temperature coefficient for growth of 1.88 (Bissinger *et al.*, 2008; Eppley, 1972).

2.6. Data analysis and mapping

The arithmetic mean of the data is reported ± the standard deviation from the mean, or as a range of minimum to maximum values. CTD measurements were binned over 1 m depth intervals. Linear correlation between two sets of measurements was calculated via Pearson's coefficient using the pearsonr function from the SciPy 0.16.1 statistical functions module, and the least-squares regression for two sets of measurements was computed using the linregress function from the SciPy statistical functions module (SciPy 0.16.1, www.scipy.org). The Data-Interpolating Variational Analysis (DIVA) gridding option in Ocean Data View (ODV4) was used to interpolate the biological, physical, and chemical data in space (Schlitzer, 2015; Troupin *et al.*, 2012). In section plots showing the relative abundance of phytoplankton groups, data points below the light compensation depth, where an insufficient number of observations in a particular population ($n<250$) were made due to insufficient sampling effort for the given population size, were removed. Since the data shown are ratios of a particular population to the sum of all populations, an insufficient number of observations in one population could have skewed the ratio estimate of individual populations.

3. Results

3.1. Overview of the transect hydrography and biogeochemistry

The transect cruise across the North Atlantic Ocean began on August 23rd, 2013 from the coast of North Carolina (USA) along the Gulf Stream, crossed the

Grand Banks, proceeded along the North Atlantic Current, and ended in the northeast (54°N 20°W) at the southern border of the subarctic Atlantic province (Figure 1 and Figure S3). The southwestern section of the transect followed the warm, saline waters of the Gulf Stream to the west of the Grand Banks (~44°W). There, the west-to-east flowing Gulf Stream extends as the North Atlantic Current at 40°W, and is directed to the eastern Atlantic basin through the transverse Charlie-Gibbs Fracture Zone (Bower and von Appen, 2008; García-Ibáñez *et al.*, 2015). The transect was characterised by zonal and meridional gradients in temperature, salinity, nutrient and PN concentrations, N isotopic composition of nitrate and PN, and phytoplankton biomass. Using these gradients we operationally grouped the stations into the southwestern stations (2-6), the shelf station (7), and the northeastern stations (8-15) (Table 1).

Sea surface temperature (SST) decreased zonally from 29.0°C at station 2 in the Gulf Stream to 13.8°C at station 15 at the border of the Atlantic subarctic province, just west of Rockall Bank (Figure 2A). Surface salinity decreased significantly from a maximum of 36.02 psu at station 4, to 32.50 psu at station 7 at the tip of the Grand Banks shelf, and rose again to a maximum of 35.38 psu at station 11 further northeast (Figure 2B). Nutrient concentrations were depleted in at least the upper 30 m of the water column throughout most of the transect (nitrate <100 nmol l^{-1}, nitrite <20 nmol l^{-1}, ammonium <50 nmol l^{-1}, phosphate <100 nmol l^{-1}; Figure 2C and Figure S4). At the northeastern stations, however, only silicate concentrations were low (332 - 779 nmol l^{-1}), while at the southwestern stations, maximum silicate concentrations ranged between 859 and 1856 nmol l^{-1} (Figure S4D). The depth of the nitracline shoaled from the southwest (max. = 101 m, station 3) to the northeast (min. = 33 m), where nitrate was at least 451 nmol l^{-1} in surface waters of the northeastern stations (12, 13, 15) (Figure 2C and Table 1). The depth of the nitracline was correlated with Z_{Ic} but not with MLD (Table 3). Nitrite maxima were typically observed between the nitracline and Z_{Ic} (except at the northeastern-most station 15, where the nitrite maximum was situated just below Z_{Ic}). Nitrite maxima ranged from 51 to 158 nmol l^{-1} at the southwestern stations, 42 nmol l^{-1}

494 near the bottom of the shelf station, and from 69 to 485 nmol l^{-1} at the northeastern
495 stations (Figure S4A).
496 The distribution of upper ocean PN mirrored the distribution of nitrate, with
497 the highest concentrations at each station observed at or just below the nitracline in
498 the southwest or in the upper mixed layer of the northeastern stations (Figure 2C
499 and Figure 3A). The concentration of PN above Z_{eu} ranged from 0.28 to 1.04 µmol l^{-1}
500 at the southwestern stations and from 0.40 to 2.35 µmol l^{-1} at the northeastern
501 stations. Occasional localised PN peaks (e.g., 3.97 µmol l^{-1} at 30 m at station 7 on the
502 Grand Banks shelf and 2.18 µmol l^{-1} at 45 m at station 8) were observed, and these
503 corresponded with occurrences of high phytoplankton biomass detected by flow
504 cytometry (see section 2.4). The distribution of POC was strongly correlated with
505 that of PN (Table 3) and the POC-to-PN molar ratio of suspended particles
506 throughout the euphotic zone had an average value of 7.3 ± 2.8 (n=33), which did
507 not show a trend with longitude or latitude (r<0.02, p>0.1).

508 **3.2. Nitrogen isotopic composition of PN and nitrate**

509 Vertical patterns in the δ^{15}N of nitrate and suspended PN provide a time-
510 integrated view of the dynamics of new production – according to the classical
511 paradigm - at each station (Figure 4). At depths shallower than the 300 nmol l^{-1}
512 nitrate isopleth, the nitrate concentration was too low for δ^{15}N determination. For
513 all profiles, the δ^{15}N of nitrate was highest at the shallowest depth for which nitrate
514 was greater than our δ^{15}N quantification threshold, and was slightly higher at the
515 northeastern stations (average of 9.4‰), compared to the southwest (average of
516 8.5‰) (Figure 4B). Evidence for nitrate assimilation, implied by the elevated δ^{15}N of
517 shallow nitrate compared to its subsurface source, was observed deeper in the
518 water column to the southwest compared to the northeast (Figure 4B). The
519 relatively low δ^{15}N of the source nitrate (below the main thermocline and Z_{lc}) in the
520 southwestern section of the transect (2.5 ± 0.1‰ at 250 m, stations 2, 3, 4 and 5)
521 compared to the source nitrate in the northeastern section (4.7 ± 0.2‰ between
522 200 and 300 m) points to different origins for this nitrate.

The $\delta^{15}N$ of PN increased from the southwest (-0.4 ± 0.4‰ at 20 m, n=5; 0.3 ± 1.1‰ for all samples above the nitracline, n=9; stations 2-6) to the northeast (4.2 ± 0.2‰ above the nitracline; stations 11, 12, 13 and 15, n=7) (Figure 4A). The mass-weighted upper ocean average $\delta^{15}N$ of PN decreased with increasing depth of the nitracline and the difference between the $\delta^{15}N$ of PN and source nitrate was less to the northeast, indicating higher nitrate reliance (Table 3; excluding shelf station 7). In general, the $\delta^{15}N$ of PN increased with depth from the shallowest sample to the waters at or below the nitracline.

3.3. Phytoplankton chlorophyll *a* biomass and community size-structure

Surface Chla concentrations were low (<0.5 mg m^{-3}) across most of the transect but increased sharply at the northeastern end (Figure 5A). The depth of the Chla maximum at each station shoaled from the southwest to the northeast, essentially following the depth of the nitracline. The depth-integrated chlorophyll (ΣChla), integrated from the surface to the light compensation depth (Z_{lc}), was also higher at the northeastern stations 13 and 15 (33.6 mg m^{-2} and 30.4 mg m^{-2}, respectively) compared to the transect average (19.1 ± 7.2 mg m^{-2}, n=12) (Figure 6). The degree to which these patterns in Chla distribution were representative of the average conditions during late summer was assessed by comparing *in situ* Chla measurements to the distribution of climatological remote sensing data for each station (Figure S5). The median [Chla] above Z_{lc} was below average (i.e., the median) for the southwestern stations and stations 7 and 8, near average for stations 9 to 12, and above average for the two northeastern-most stations 13 and 15. The higher-than-expected [Chla] at the two northeastern-most stations is thus indicative of summer bloom conditions.

Throughout the transect, most of the ΣChla was contained in the pico (<2 μm) (78 ± 13%, n=12) and nano sized-fractions (2-20 μm) (20 ± 11%, n=12). The proportion of Chla in the micro sized-fraction (>20 μm) was very low on average (3 ± 2%, n=12) (Figure 6). The northeastern stations (12, 13 and 15), together with the shelf station 7, were characterised by the highest contribution of

552 nanophytoplankton (up to 36% at station 13) and microphytoplankton (up to 8% at
553 station 7) to ΣChla.

554 **3.4. Pico- and nanoplankton abundance and biomass**

555 The abundance and biomass of pico- and nanoplankton were determined by
556 flow cytometry in order to produce a more detailed description of phytoplankton
557 community diversity and to assess the biomass distribution of each phytoplankton
558 group, avoiding the confounding effect of light intensity that complicates
559 interpretation of the complementary size-fractionated Chla measurements. At the
560 southwestern stations, *Prochlorococcus* cells numerically dominated the
561 phytoplankton community yet *Prochlorococcus* was not detected at the shelf and
562 northeastern stations (Figure S6A). Maximum cell concentrations at the
563 southwestern stations were observed deep in the euphotic zone, above or just
564 below the nitracline (0.86 - 1.24 × 10^6 cells ml^{-1}), as well as in the upper 20 m of the
565 water column at stations 5 and 6 (0.86 - 1.44 × 10^5 cells ml^{-1}). *Synechococcus* was
566 present throughout the transect although cell concentrations were low in the
567 southwestern section, increasing towards the northeast. At the southwestern
568 stations the highest abundance of this group was mostly confined to the upper 20 m
569 (0.80 ± 0.13 × 10^4 cells ml^{-1}, n=9), except at station 6 where the maximum
570 abundance was observed just above the nitracline (63 m; 2.30 × 10^4 cells ml^{-1}).
571 *Synechococcus* cells were most abundant in the nitracline at the shelf station 7 and
572 station 8, and at the surface of the northeastern station 13 (5.32 - 7.19 × 10^4 cells ml^{-1}) (Figure S6B). The abundance of picoeukaryotes and nanoeukaryotes was lower in
574 the southwestern part of the transect, with maxima at or below the nitracline
575 (picoEuks: 4.4 ± 2.3 × 10^3 cells ml^{-1}; nanoEuks: 0.6 ± 0.3 × 10^3 cells ml^{-1}), compared
576 to the shelf and the northeastern stations (picoEuks: 9.8 ± 6.7 × 10^3 cells ml^{-1};
577 nanoEuks: 3.1 ± 1.6 × 10^3 cells ml^{-1}) (Figures S6C and S6D). In the
578 nanophytoplankton size group, the noPE-nanoEuk population was by far the most
579 numerically abundant group (94 ± 6% of total nanophytoplankton cells). The cell
580 abundance of the other nanophytoplankton groups, Cocco and PE-nanoEuk, was
581 very low across the entire transect (<0.1 × 10^3 cells ml^{-1}, <0.4 × 10^3 cells ml^{-1}),

582 although PE-nanoEuk cells constituted up to 20% of all nanophytoplankton cells at
583 station 6 (data not shown).
584 Because of large differences in cell size, the total biomass distribution of
585 populations determined from biovolume estimates (Figures 5B and 7) is distinct
586 from the patterns of Chla and cell abundance outlined above (Figures 6A and S6).
587 *Prochlorococcus* contributed up to 0.47 ± 0.12 μmol C l^{-1} or 46 ± 7% (n=5) of the
588 combined pico- and nanophytoplankton carbon biomass at their depth maxima at
589 the southwestern stations (Figures 7A and 8A). The biomass concentrations of
590 *Synechococcus* and picoeukaryotes were of the same order of magnitude (Figures 7B
591 and 7C), with maxima ranging from 0.10 to 0.27 μmol C l^{-1} and 0.16 to 0.42 μmol C l^{-1}
592 at the southwestern stations, and from 0.15 to 0.85 μmol C l^{-1} and 0.21 to 1.04 μmol
593 C l^{-1} at the shelf and northeastern stations. Nanoeukaryote biomass at the
594 southwestern stations was lower than at the shelf and northeastern stations. At
595 their depth maxima, nanoeukaryotes biomass ranged from 0.32 to 0.84 μmol C l^{-1} in
596 the southwest, from 1.04 to 5.33 μmol C l^{-1} in the northeast, and had a localised peak
597 of 8.63 μmol C l^{-1} at the shelf station (30 m) (Figure 7D). Cyanobacteria dominanted
598 the picophytoplankton biomass in the southwestern section (76 ± 14%, n=27)
599 compared to the northeastern stations (37 ± 20%, n=38) in the upper 125 m of the
600 water column (Figures 8A and 8B).
601 The vertical distribution of picophytoplankton biomass showed group-
602 specific trends. The picoeukaryote populations made up a relatively greater
603 proportion of the pico- and nanophytoplankton biomass (17.0 ± 7.9%, n=20) at the
604 depths near the nitracline (when present) compared to *Synechococcus* (9.2 ± 7.7%,
605 n=20) (Figures 8B and 8C). *Synechococcus* populations, on the other hand, were
606 mostly confined to the better-lit shallower water column (18.4 ± 9.0%, n=27), where
607 the relative contribution of picoeukaryotes was lower (8.9 ± 5.0%, n=27 not
608 adjacent to the nitracline).
609 The nanoeukaryote phytoplankton made up a substantial portion of the pico-
610 and nanophytoplankton biomass despite their relatively low cell numbers,
611 contributing 40 ± 11% (n=23) of the biomass at the southwestern stations, and 69 ±
612 11% (n=39) at the shelf and northeastern stations in the upper 125 m of the water

column (in instances where a representative population sample of at least 250 nanophytoplankton cells were counted) (Figures 8D and S6D). The distribution of the nanophytoplankton biomass was heterogeneous, with low concentrations in the euphotic zone in the southwestern part of the transect (0.34 ± 0.19 µmol C l^{-1}, n=22), localised maxima at stations 7 and 8 (8.63 and 3.81 µmol C l^{-1}), and high concentrations in the upper mixed layer of the northeastern stations 12, 13 and 15 (3.23 ± 1.18 µmol C l^{-1}, n=9) (Figure 7D).

The average cellular carbon content for the picoeukaryotes and combined nanoeukaryote phytoplankton groups was 64 ± 16 fmol C $cell^{-1}$ (n=73) and 741 ± 247 fmol C $cell^{-1}$ (n=68, excluding station 7), respectively, corresponding reasonably well to the values reported by (Tarran *et al.*, 2006) for picoeukaryotes (36.7 fmol C $cell^{-1}$) and total nanoeukaryotes (763 fmol C $cell^{-1}$) in the Northeast Atlantic in early summer. Noteworthy was the larger cellular biomass of total nanoeukaryotes (1585 ± 537 fmol C $cell^{-1}$, n=8) in the cold, low salinity waters at the shelf station 7 compared to the rest of the transect. The flow cytometry-derived phytoplankton biomass (FCM phyto C, µmol C l^{-1}) explained 73% of the variance in POC concentration (µmol C l^{-1}) across the transect, and the deviation from a one-to-one relationship between both measures of biomass (log_{10}[POC] = 0.81 × log_{10}[FCM phyto C] + 0.64, n=36, $p<0.001$) points to either an underestimate of total phytoplankton biomass by FCM phyto C or to the contribution of non-phytoplankton particles, such as heterotrophs and detritus, to the POC.

Finally, the cell abundance of heterotrophic bacteria over the upper 125 m ranged from 0.10 - 1.66 × 10^6 cells ml^{-1}, generally decreasing with depth (Figure S7), and this was positively correlated with total Chla, FCM phyto C and the rate of inorganic carbon fixation (ρDIC, µmol C l^{-1} h^{-1}) (see section 3.5) (Table 3). These strong correlations suggest a close coupling between the phototrophic and heterotrophic components of the microbial food web.

3.5. Primary production and phytoplankton turnover rate

The activity of the phytoplankton standing stocks was estimated by measuring the inorganic carbon fixation rate (i.e., primary production; ρDIC, µmol C

643 l^{-1} h^{-1}) at each transect station at three irradiance levels within the euphotic zone.
644 Carbon fixation rates (n=36) ranged from 0.009 µmol C l^{-1} h^{-1} at the base of the
645 euphotic zone in the oligotrophic surface waters in the southwest, to 0.132 µmol C l^{-1} h^{-1} at the subsurface biomass peak in the colder Grand Bank shelf water (30 m,
647 station 7), and then up to 0.222 µmol C l^{-1} h^{-1} during the summer phytoplankton
648 bloom at the northeastern-most station 15 (Figure 9A). The ρDIC showed a positive
649 relationship with the different measures of biomass: [POC], [Chla] and FCM phyto C
650 across the transect and light depths (Table 3).

651 The turnover rate of phytoplankton biomass (*V*DIC, h^{-1}), obtained by
652 normalizing the carbon fixation rates to [FCM phyto C], ranged from 0.012 to 0.086
653 h^{-1} and was generally slowest at the deepest light depth (Figure 9B). Across the
654 transect, *V*DIC was positively correlated with *in situ* temperature (Table 3). The
655 phytoplankton community composition could partly explain the variation in *V*DIC,
656 as it was negatively correlated with the proportion of nanophytoplankton FCM
657 carbon biomass (Table 3). However, this is likely at least partly due to the negative
658 correlation between the proportion of nanophytoplankton FCM carbon biomass and
659 *in situ* temperature (Table 3).

660 4. Discussion

661 4.1. Late summer hydrography and biogeochemistry in the North Atlantic

662 The zonal/meridional transect crossed several biogeographical provinces
663 (Gulf Stream (GFST), Northwest Atlantic shelves (NWCS), North Atlantic Drift
664 (NADR), and the southern border of the Atlantic subarctic province (SARC)) (Figure
665 1) (Longhurst (2007), Reygondeau *et al.* (2013), G. Reygondeau, personal
666 communication 2014). The broad patterns in temperature, Z_{eu} and the horizontal
667 and vertical distribution of Chla were representative of the classical biogeographical
668 provinces described by Longhurst (2007) for the locations sampled during late
669 summer (World Ocean Atlas 2013 (WOA13), August-September;
670 https://www.nodc.noaa.gov/OC5/woa13/pubwoa13.html). A large part of the
671 southwestern section of the transect followed the Gulf Stream, which was

characterised by high SST (>23 °C). The transect stations did not intersect any mesoscale eddies, as seen from the surface velocity fields (Figure S3), but the cruise track did traverse sub-mesoscale fronts characterised by sharp changes in surface temperature and salinity (Figure S8). At station 8, for example, the SST was ~2.5-3.0 °C warmer than at adjacent (24 - 39 km) stations. The depleted surface nutrient concentrations throughout the transect were typical for the late summer (nitrate 0-2.00 μmol l^{-1}, phosphate 0.03-0.30 μmol l^{-1}, silicate 0.06-3.00 μmol l^{-1}; WOA13, August-September, upper 25 m). The low Chla concentrations throughout the transect (median $[Chla]_{Zlc}$ per station range 0.09-0.34 mg m^{-3}) were characteristic or lower-than-expected for the regions and/or the time of year (e.g., the Gulf Stream and Grand Banks shelf), with the exception of the summer bloom conditions observed at the two northeastern-most stations (median $[Chla]_{Zlc}$ range 0.66-0.74 mg m^{-3}) (Figure S5).

4.2. Phytoplankton community composition from the Gulf Stream to the subarctic Atlantic

The biogeochemical gradients along the zonal/meridional North Atlantic transect were reflected in the phytoplankton community composition. The biomass and cell abundance of late summer phytoplankton communities throughout the transect (GFST - SARC) were strongly dominated by pico- and nanophytoplankton groups. Microphytoplankton biomass, based on size-fractionated Chla, constituted only a minor part of the summer phytoplankton communities. The lack of significant microphytoplankton Chla even at the northeastern summer bloom stations (Figure 6) may be a consequence of insufficient silicate replenishment in the case of diatoms, or slow growth response time and sensitivity to increased turbulence in the case of phototrophic dinogflagellates (Barton *et al.*, 2015; Irwin *et al.*, 2012). The patterns in pico- and nanophytoplankton community size-structure and low levels of biomass were consistent with the few available summer field observations for the region using either flow cytometry (Buck *et al.*, 1996; Li, 1995; Li and Harrison, 2001) or pigment-based approaches (Dandonneau *et al.*, 2004).

701 The maximum cell abundance of *Prochlorococcus* at the southwestern
702 stations in this study was comparable to that observed by flow cytometry in surface
703 waters of the western North Atlantic in August and September (~0.5-1 × 10^5 ml^{-1};
704 Casey *et al.* (2007); DuRand *et al.* (2001)), the eastern North Atlantic (35°N 23°W) in
705 September (~1 × 10^5 ml^{-1}) (Zinser *et al.*, 2006) and in the Gulf Stream (~6 × 10^4 ml^{-1}
706 at ~37°N ~69°W; ~1.2 × 10^5 ml^{-1} at ~42°N ~55°W) in June and September
707 (Cavender-Bares *et al.*, 2001; Li, 1995). The lack of *Prochlorococcus* cells from the
708 Grand Banks (~44°N) northwards is consistent with its average geographical
709 distribution and preference for warmer water (at least ~12 °C) (Partensky *et al.*,
710 1999b).
711 The detection of *Synechococcus* populations throughout the transect is in
712 accordance with the cosmopolitan distribution of this genus (Partensky *et al.*,
713 1999a). Relatively higher contributions of *Synechococcus* to the pico- and
714 nanophytoplankton biomass were measured near the surface at the southwestern
715 stations as well as in lower salinity surface waters of the shelf and adjacent station,
716 consistent with the genus' reported niche breadth (Partensky *et al.*, 1999a;
717 Zwirglmaier *et al.*, 2008). *Synechococcus* reached its highest cell abundance at the
718 northeastern summer bloom station 13 (7.19 × 10^4 cells ml^{-1}) where nitrate had
719 likely been recently resupplied. These higher cell concentrations are comparable to
720 those measured by Buck *et al.* (1996) and Heywood *et al.* (2006) during a summer
721 transect (~2 × 10^4 - 1 × 10^5 cells ml^{-1}, from 45°N-60°N) and may have been
722 stimulated by the higher nitrate concentrations (Glover *et al.*, 2007; Glover *et al.*,
723 1988) (see below).
724 Picoeukaryote phytoplankton were a ubiquitous feature of the plankton
725 community throughout the transect and, based on their biomass distribution,
726 contributed significantly to Chla in the picophytoplankton size-group, together with
727 their cyanobacterial counterparts (Figures 6, 7, and 8). This extensive geographical
728 distribution may reflect the high taxonomic diversity within this group (Grob *et al.*,
729 2011; Kirkham *et al.*, 2013). The exception to the ubiquitous presence of the
730 picoeukaryotes was their relative absence at the Grand Banks shelf station where
731 they were replaced by *Synechococcus* and nanophytoplankton. In general,

732 picoeukaryote phytoplankton contributed relatively more to biomass deeper in the
733 water column, closer to the nitracline. Such a vertical distribution pattern seems to
734 be a consistent feature of this flow cytometrically-defined group across different
735 environments (Buck *et al.*, 1996; Cabello *et al.*, 2016; Painter *et al.*, 2014; Tarran *et*
736 *al.*, 2006). When nitrate was available near the surface, such as at the northeastern
737 summer bloom stations, picoeukaryote biomass was still relatively more abundant
738 closer to the base of the euphotic zone even though this group had a higher biomass
739 throughout the water column compared to the southwestern section of the transect.
740 The main trend in the distribution of nanophytoplankton was a higher
741 contribution to the total phytoplankton biomass from the Grand Banks shelf to the
742 northern part of the NADR province compared to the Gulf Stream stations (Figures
743 6, 7, and 8). This trend coincided with the northeastward shoaling of the nitracline
744 along the transect. The patchiness of nanophytoplankton biomass corresponded to
745 localised increases in nutrient and light availability (e.g., station 7, 13 and 15),
746 suggesting that this size-group may respond more strongly to the alleviation of
747 nutrient limitation (e.g., nitrate), or be under looser top-down control than smaller-
748 sized phytoplankton. At the northeastern-most summer bloom station, calcified
749 coccolithphore cells did not contribute significantly to the nanophytoplankton
750 biomass (<~14 μm) although late summer coccolithophore blooms have been
751 documented quite regularly north of the subpolar front (52-54°N) (Holligan *et al.*,
752 1993; Longhurst, 2007), which is at the northern boundary of our transect. North of
753 that area and in the absence of a coccolithophore bloom, the majority of summer
754 phytoplankton community biomass (mean euphotic zone [Chla]= 0.41 mg m^{-3}) has
755 been observed to comprise of small flagellates (picoeukaryotes (18%),
756 nanoeukaryotes (68%) and Cocco (6%)), with only minor contributions from
757 *Synechococcus* (7%) and diatoms (1%) (Poulton *et al.*, 2010). This is comparable to
758 the phytoplankton community composition we observed at the northeastern end of
759 our transect.

4.3. Imprint of phytoplankton nitrogen utilisation on the nitrogen isotopes

The increase in the $\delta^{15}N$ of surface suspended PN along the path of the Gulf Stream and the North Atlantic Current, from ~0‰ in the southwest to ~5‰ in the northeastern part of the transect, is a first order reflection of the isotopic composition of the subsurface nitrate source, the degree to which this nitrate is consumed by phytoplankton, and the extent of phytoplankton reliance on other N forms relative to subsurface nitrate. However, variations in the degree of consumption of the supplied nitrate are unlikely to be an important driver of the $\delta^{15}N$ of surface suspended PN at most stations because the isotope effect of nitrate assimilation is not expressed when nitrate is completely consumed (i.e., surface nitrate concentration was <100 nmol l^{-1} at all stations except 12, 13 and 15) (Figure 2C).

Regarding the subsurface nitrate source, the basin-scale signal of N_2 fixation is evident as a "bolus" of low-$\delta^{15}N$ nitrate (~2.5 ± 0.1‰) in the thermocline (~200-400 m) of the southwestern stations (Figure 4B; Knapp *et al.* (2008)). However, N_2 fixation need not be occurring *in situ* to produce this signal. Rather, its isotopic imprint is advected and integrated into subtropical thermocline waters on the timescale of decades through the remineralisation of low-$\delta^{15}N$ PN deriving from N_2 fixation elsewhere in the basin (Knapp *et al.*, 2005). By contrast, the higher $\delta^{15}N$ of subsurface nitrate at the northeastern stations (4.7 ± 0.2‰) is similar to the mean $\delta^{15}N$ of deep ocean nitrate (~5‰; Sigman *et al.* (2000)), and derives from the combined influence of Mediterranean Water, North Atlantic Central Water, and Subpolar Mode Water (Talley, 2011).

In contrast to the $\delta^{15}N$ of subsurface nitrate, which ranged from 2.4‰ to 5.1‰ along the transect, N_2 fixation and atmospheric N deposition introduce low-$\delta^{15}N$-N to surface waters (-5‰ to 0‰; Carpenter *et al.* (1997); Knapp *et al.* (2008); Minagawa and Wada (1986)). However, studies conducted near our southwestern stations suggest that, on an annual basis, fluxes from both sources are too low to account for the low $\delta^{15}N$ of PN in this region (Altabet, 1988; Knap and Jickells, 1986; Knapp *et al.*, 2008; Knapp *et al.*, 2005; Michaels *et al.*, 1993). Instead, the low-$\delta^{15}N$

790 PN to the southwest of the transect is best interpreted as the result of upper ocean N
791 recycling (Altabet, 1988; Fawcett *et al.*, 2011; Fawcett *et al.*, 2014; Treibergs *et al.*,
792 2014): Zooplankton sustained by upper ocean PN metabolise and excrete ^{15}N-
793 depleted ammonium, the assimilation of which renders phytoplankton (i.e., PN) low
794 in δ^{15}N (Checkley and Miller, 1989; Montoya *et al.*, 2002). The apparently stronger
795 reliance on regenerated N to the southwest of the transect, as implied by the δ^{15}N of
796 PN, is consistent with the observed depletion of the surface nitrate pool in this
797 region (Figure 2C).
798 From the Grand Banks shelf to the northeastern end of the transect near the
799 subarctic Atlantic, the δ^{15}N of PN gradually increases (Figure 4A), reflecting
800 increased reliance on subsurface nitrate as well as a higher δ^{15}N for the nitrate
801 supply (Figure 4B). However, removing the potentially confounding effect of
802 subsurface nitrate δ^{15}N does not remove the clear pattern of increasing PN δ^{15}N and
803 thus increasing dependence on nitrate relative to regenerated N from the Gulf
804 Stream to the southwest to the subarctic Atlantic to the northeast (Figure 10).
805 Stations 8 and 9, although having a similar fraction of nanophytoplankton biomass
806 as the more northeastern stations, had SST and SSS properties that were different
807 from stations further northeast (Figure S8), indicating mixing with fresher water
808 masses. This could cause the misidentification of the nitrate source and thus an
809 overcorrection of the surface δ^{15}N-PN (Figure 10, central diamond pair, Table 3).
810 The increased reliance on subsurface nitrate inferred from the zonal rise in δ^{15}N-PN
811 is reflected in the increased biomass contribution of nanoeukaryotes and decreased
812 biomass contribution of picocyanobacteria to the phytoplankton community, from
813 the Gulf Stream to subarctic Atlantic part of the transect (Figure 10 and Table 3).
814 One caveat to the above is that using the δ^{15}N of bulk suspended PN to assess
815 autotrophic N assimilation patterns is not ideal since PN also contains heterotrophic
816 and detrital biomass N, which have different δ^{15}N signatures (Fawcett *et al.*, 2011).
817 For example, the rise in δ^{15}N-PN below the nitracline at all stations from which we
818 have sufficiently deep data (Figure 4A and S9) likely indicates a contribution of

819 degraded detrital PN, which is high in $\delta^{15}N$ due to the preferential remineralization
820 of ^{14}N by heterotrophic bacteria (Altabet and McCarthy, 1986; Möbius, 2013).
821 Nitrate was easily detectable throughout surface waters of the northern
822 extent of the NADR (stations 13 and 15, Figure 2C), such that the isotope
823 discrimination during nitrate assimilation needs to be considered when inferring
824 phytoplankton reliance on nitrate versus regenerated N from the $\delta^{15}N$ of suspended
825 PN. Station 12 is excluded from this analysis because we have only two euphotic
826 zone measurements of nitrate >300 nmol l^{-1}, both of which are below the MLD.
827 During nitrate assimilation, phytoplankton preferentially consume ^{14}N-bearing
828 nitrate, leaving the ambient nitrate pool enriched in ^{15}N (Sigman *et al.*, 1999; Wada
829 and Hattori, 1978). Algal nitrate consumption thus elevates the $\delta^{15}N$ of subsurface
830 nitrate supplied to the euphotic zone by upward vertical mixing. The phytoplankton
831 PN produced from the consumption of this nitrate is lower in $\delta^{15}N$ than the nitrate
832 itself due to the isotopic fractionation that occurs during its assimilation; this is
833 quantified by the isotope effect, ε_{assim} (ε_{assim}, in ‰ vs. N_2 in air, = $(^{14}k/^{15}k - 1) \times$
834 1000, where ^{14}k and ^{15}k are the rate coefficients of the reaction for ^{14}N- and ^{15}N-
835 containing nitrate, respectively). The $\delta^{15}N$ of PN increases with increasing surface
836 ocean nitrate consumption (Altabet and Francois, 1994), ultimately approximating
837 the $\delta^{15}N$ of the source nitrate upon complete nitrate consumption. We used the
838 Rayleigh model to estimate ε_{assim} from the vertical profiles of nitrate concentration
839 and $\delta^{15}N$, which can then be used to predict the $\delta^{15}N$ of PN produced from the
840 assimilation of nitrate with a source concentration and $\delta^{15}N$ equal to that measured
841 at each station (Figure S9A-D; Suppl. Text 1).
842 At both stations, the $\delta^{15}N$ of suspended PN from the mixed layer is very
843 similar to the integrated product $\delta^{15}N$ predicted by the Rayleigh model (Figure S9,
844 Suppl. Text 1), suggesting a strong reliance on nitrate by the community. The
845 elevated surface nitrate concentration at station 15 could be due to its location close
846 to the margin of the subpolar gyre, where the unused nitrate concentration tends to
847 be higher than in the rest of the basin at this time of year (WOA 2013; cf. Fig. 2b in
848 Straub *et al.* (2013)). As such, the nitrate supply could have been advected from this

perennial high-nutrient region to the northwest. However, nitrate appears to have been recently (on the order of days to a week) resupplied to the surface at station 15 as suggested by *in situ* [Chla], which was two times higher than expected compared to remote sensing climatology for this area (Figure S5), and the relatively high primary production rate (~2 μmol l^{-1} d^{-1}). Moreover, the mass-weighted $\delta^{15}N$ of PN in the upper mixed layer is higher (4.3‰) than that predicted by the integrated product of the Rayleigh model (~3‰; Figure S9D, integrated product); this may reflect a contribution of PN produced prior to the bloom, which had a $\delta^{15}N$ of ~5‰ due to complete consumption of the subsurface nitrate supply. The $\delta^{15}N$ of the PN sampled during the cruise may not yet have been altered significantly by the consumption of lower-$\delta^{15}N$, newly-supplied nitrate.

High $\delta^{15}N$-PN may also reflect a significant contribution from rapidly growing phytoplankton (i.e., nanoeukaryotes; Figures 7D and 10A) with a $\delta^{15}N$ that is more similar to the Rayleigh model's instantaneous product than integrated product, since growing phytoplankton integrate over only a short period of time and thus a short degree of nitrate consumption (Fawcett *et al.*, 2011). Nitrate was present at concentrations >2 μmol l^{-1} throughout the mixed layer at station 15, with a $\delta^{15}N$ ranging from 6.3‰ to 11‰. Consumption of this nitrate would produce instantaneous product biomass with an average $\delta^{15}N$ of 5.9‰; including some portion of this in the suspended PN pool could easily elevate its $\delta^{15}N$ above that of the predicted integrated product.

One final consideration is the potential effect of euphotic zone nitrification on the $\delta^{15}N$ of nitrate and PN. As described above, the co-occurrence of ammonium assimilation and nitrification will result in the production of low-$\delta^{15}N$ regenerated nitrate, rendering it indistinguishable from other recycled N forms, and distinct from subsurface nitrate (DiFiore *et al.*, 2009; Fawcett *et al.*, 2011). Thus, even if euphotic zone nitrification were occurring, $\delta^{15}N$-PN would still accurately record the extent of new relative to regenerated production over most of the transect.

However, at the stations with relatively high upper ocean nitrate concentrations (12, 13, and 15), euphotic zone PN produced from regenerated

879 nitrate assimilation could be mistaken for PN produced by the assimilation of
880 subsurface nitrate with an isotope effect. Since regenerated nitrate will be
881 assimilated with the same ε_{assim} as subsurface nitrate, the fact that mixed layer δ^{15}N-
882 PN is well predicted by the Rayleigh model does not rule out the possibility that
883 some fraction of the nitrate being assimilated was produced in the euphotic zone.
884 This can be addressed using the oxygen (O) isotopes of nitrate (δ^{18}O, in ‰ vs.
885 VSMOW) in conjunction with the N isotopes. Briefly, co-occurring nitrate
886 assimilation and nitrification causes samples to fall above a 1:1 line in nitrate δ^{15}N
887 vs. δ^{18}O space, whereas nitrate assimilation alone results in samples falling on the
888 1:1 line (Sigman *et al.*, 2005; Wankel *et al.*, 2007; Suppl. Text 2.2). Evaluation of the
889 coupled N and O isotopes of nitrate at the northeastern-most stations reveals a 1:1
890 relationship in the upper 100 m (Figure S9E-F), strongly indicating that euphotic
891 zone nitrification is insignificant relative to the upward transport of subsurface
892 nitrate. In sum, the PN and nitrate isotope data suggest near-complete reliance of
893 the phytoplankton community on subsurface nitrate in the mixed layer of the
894 northeastern-most stations, consistent with a zonal pattern of increasing new
895 production from the Gulf Stream to the southwest to subarctic Atlantic to the
896 northeast of the transect.
897 The dominance of cyanobacterial picoplankton biomass in the Gulf Stream
898 together with the isotopic evidence for high reliance on recycled N (Figure 10B)
899 suggests that their ecological strategy is in exploiting these N forms in oligotrophic
900 environments (Fawcett *et al.*, 2011; Zubkov *et al.*, 2003). Culture studies have
901 shown that all ecotypes of *Prochlorococcus* grow well on ammonium (e.g., Moore *et*
902 *al.*, 2007; Moore *et al.*, 2002), most can utilise urea, and some low-light strains will
903 grow on nitrite (Moore *et al.*, 2002). Only recently has there been a report of nitrate
904 assimilation by cultured ecotypes (Berube *et al.*, 2015) but their importance in the
905 ocean remains unknown. This is thought to be due to a lack of the genetic machinery
906 for nitrate reduction (Dufresne *et al.*, 2003; Moore *et al.*, 2002), which is an
907 energetically expensive process. There have been very few direct studies of the
908 nutritional ecology of *Prochlorococcus* in the field (Casey *et al.*, 2007; Li, 1994;

909 Martiny *et al.*, 2009; Zubkov *et al.*, 2003). Zubkov *et al.* (2003; 2005) reported high
910 *in situ* rates of organic N assimilation by marine cyanobacteria in the Arabian Sea
911 and South Atlantic subtropical front, and attributed 33% of the total bacterial
912 turnover of amino acids to *Prochlorococcus*, suggesting that this allows them to
913 dominate over other autotrophs and heterotrophic bacteria in oligotrophic waters.
914 While there is some evidence that certain strains of *Prochlorococcus* may be able to
915 use nitrate in the environment (Casey *et al.*, 2007; Martiny *et al.*, 2009; Treibergs *et*
916 *al.*, 2014), their overwhelming preference appears to be for reduced N forms. This,
917 coupled with their extremely high affinity for phosphate in the open ocean (Lomas
918 *et al.*, 2014), underscores the adaptation of this organism to chronically oligotrophic
919 environments (Moore *et al.*, 2002; Scanlan and Post, 2008) and explains their
920 dominance to the southwest of the transect.
921 The congruence between the N isotopes and the distribution of *Synechococcus*
922 along the transect is less straightforward and probably originates from the ecotype
923 diversity of this genus (Zwirglmaier *et al.*, 2008). Indeed, *Synechococcus* is the most
924 ubiquitous photoautotroph in the ocean, and has been found in virtually every
925 marine environment (Campbell *et al.*, 1997; Olson *et al.*, 1990; Partensky *et al.*,
926 1996). Although often discussed in the context of the subtropical ocean gyres,
927 *Synechococcus* tends to be more numerically abundant in nutrient-rich rather than
928 oligotrophic environments (Partensky *et al.*, 1999a; Scanlan, 2003), which is
929 consistent with our observations (Figure S6B). Cultured marine *Synechococcus*
930 species have been reported to utilise ammonium, nitrite, nitrate, urea, and amino
931 acids (Collier *et al.*, 1999; Glibert *et al.*, 1986; Lindell *et al.*, 1998; Moore *et al.*, 2002;
932 Paerl, 1991), and under severe N deprivation, some strains will even degrade their
933 phycoerythrin protein-pigment complex as an internal N source (Kana *et al.*, 1992;
934 Wyman *et al.*, 1985). With the exception of three recent isolates from the Red Sea
935 that cannot assimilate nitrate (Fuller *et al.*, 2003), all studied strains of
936 *Synechococcus* can utilise both nitrate and nitrite as their sole N source (Bird and
937 Wyman, 2003; Moore *et al.*, 2002). In the environment, *Synechococcus* growth rates
938 correlate with ambient nitrate concentrations (Blanchot *et al.*, 1992; Partensky *et*
939 *al.*, 1999a), and natural populations of *Synechococcus* appear to respond to periodic

940 nitrate inputs (DuRand *et al.*, 2001; Glover *et al.*, 1988). The ability to assimilate
941 both oxidised and reduced N forms may reflect a higher cellular N requirement,
942 especially given the large, N-rich light-harvesting protein complexes
943 (phycobilisomes) that must be maintained (Scanlan, 2003). This could explain the
944 predominance of *Synechococcus* shallower in the water column (Figures 7B and 8B)
945 as the low light levels at the base of the euphotic zone may not yield sufficient
946 energy to reduce oxidised N forms. In any case, our data are consistent with the
947 competitive advantage of *Synechococcus* being its cosmopolitan nutritional ecology.
948 Isotopic evidence for nitrate assimilation near the nitracline appears to be
949 associated with a higher relative abundance of picoeukaryote phytoplankton
950 biomass at this depth, suggesting that picoeukaryotes, despite their small mean cell
951 size (<2.5 μm), are important drivers of new production across the transect (Figure
952 8C). This is consistent with studies by Fawcett et al. (2011; 2014) and Painter *et al.*
953 (2014) that demonstrated the importance of this phytoplankton group to new and
954 export production in the oligotrophic North Atlantic, due to their apparent affinity
955 for nitrate even when ambient concentrations are extremely low, as well as their
956 position deeper in the water column near the nitracline. In contrast to the
957 picoeukaryotes and consistent with the observations of Painter *et al.* (2014), in this
958 study the nanoeukaryotic phytoplankton contribution to biomass was most
959 important when nitrate was available near the surface or had been fairly recently
960 supplied (Figure 10A). This appears to have been the case at the two northeastern-
961 most stations where the δ^{15}N of nitrate was high throughout euphotic zone waters
962 (indicating partial nitrate consumption), and may point to a growth response by
963 nanoeukaryote phytoplankton groups and an increased reliance on nitrate when it
964 is abundant. Measurements of the δ^{15}N of flow-sorted phytoplankton groups would
965 help to clarify their various nutritional niches and further our understanding of the
966 role of community composition and structure in the marine nitrogen cycle across
967 biogeochemical regimes.

5. Conclusions

Phytoplankton play a pivotal role in the cycling of energy and elements through the ocean's food webs, and so determine both the strength and efficiency of the biological pump. The broad metabolic (e.g., (in)ability for nitrate uptake) and morphological (e.g., cell size) diversity in phytoplankton species often translates into different biogeochemical functions (e.g., with regard to export production). This study captured an ocean basin-scale gradient in surface N utilisation in oligotrophic to mesotrophic regimes, from the subtropical North Atlantic along the Gulf Stream and the North Atlantic Current up to the southern boundary of the subarctic Atlantic. Increasing ecosystem reliance on subsurface nitrate (i.e., classical new production), inferred from N species concentration measurements and the N isotopic composition of PN and nitrate from this summer transect, was associated with the shoaling of the nitracline from the Gulf Stream to the subarctic Atlantic. This broad zonal pattern in autotrophic nitrate assimilation was reflected in changes in the composition of the phytoplankton assemblage, as indicated by the distinct distribution of phytoplankton group-specific contributions to Chla and carbon biomass, found between biogeochemical provinces. This is consistent with the differential N assimilation capabilities of the dominant phytoplankton groups in each region, as well as with variations in the rate of nitrate supply to the photic zone from the subtropics to the temperate oceanic provinces. Identification of the phytoplankton groups that assimilate nitrate using a combination of flow cytometric sorting and N isotope analysis would shed further light on the relationship between phytoplankton diversity and N cycling in the ocean, opening up the suspended PN "black box" to further mechanistic and ecological understanding.

6. Acknowledgements

- The captain and crew of the R/V Endeavor for their professionalism

- Jeff Hoffman (JCVI) and Keiran Swart for assistance with CTD deployment and sampling
- Sean McIntee for help with flow cytometric analyses
- Heidi Sosik and her lab for providing the materials and data for the intercalibration of flow cytometric forward scatter and biovolume relationships
- Gabriel Reygondeau for attributing the sampling stations to dynamic biogeochemical provinces
- National Science Foundation grant n°OCE-1136345 for funding B. B. Ward and D. M. Sigman.
- The two anonymous reviewers for their helpful comments and suggestions, which helped to improve this manuscript.

7. References

Alkire, M., Lee, C., D'Asaro, E., Perry, M., Briggs, N., Cetinić, I., Gray, A., 2014. Net community production and export from Seaglider measurements in the North Atlantic after the spring bloom. Journal of Geophysical Research: Oceans 119 (9), 6121-6139.

Altabet, M., 1988. Variations in nitrogen isotopic composition between sinking and suspended particles: Implications for nitrogen cycling and particle transformation in the open ocean. Deep Sea Research Part A. Oceanographic Research Papers 35 (4), 535-554.

Altabet, M.A., Francois, R., 1994. Sedimentary nitrogen isotopic ratio as a recorder for surface ocean nitrate utilization. Global Biogeochemical Cycles 8, 103-116.

Altabet, M.A., McCarthy, J.J., 1986. Vertical patterns in 15N natural abundance in PON from the surface waters of warm-core rings. Journal of Marine Research 44 (1), 185-201.

Altieri, K.E., Fawcett, S.E., Peters, A.J., Sigman, D.M., Hastings, M.G., 2016. Marine biogenic source of atmospheric organic nitrogen in the subtropical North Atlantic. Proceedings of the National Academy of Sciences 113 (4), 925-930.

Azam, F., Fenchel, T., Field, J.G., Gray, J.S., Meyerreil, L.A., Thingstad, F., 1983. The ecological role of water-column microbes in the sea. Marine Ecology-Progress Series 10 (3), 257-263.

Barton, A.D., Finkel, Z.V., Ward, B.A., Johns, D.G., Follows, M.J., 2013. On the roles of cell size and trophic strategy in North Atlantic diatom and dinoflagellate communities. Limnology and Oceanography 58 (1), 254-266.

Barton, A.D., Lozier, M.S., Williams, R.G., 2015. Physical controls of variability in North Atlantic phytoplankton communities. Limnology and Oceanography 60 (1), 181-197.

Bertilsson, S., Berglund, O., Karl, D.M., Chisholm, S.W., 2003. Elemental composition of marine *Prochlorococcus* and *Synechococcus*: Implications for the ecological stoichiometry of the sea. Limnology and Oceanography 48 (5), 1721-1731.

Berube, P.M., Biller, S.J., Kent, A.G., Berta-Thompson, J.W., Roggensack, S.E., Roache-Johnson, K.H., Ackerman, M., Moore, L.R., Meisel, J.D., Sher, D., 2015. Physiology and evolution of nitrate acquisition in *Prochlorococcus*. The ISME journal 9 (5), 1195-1207.

Bird, C., Wyman, M., 2003. Nitrate/nitrite assimilation system of the marine picoplanktonic cyanobacterium Synechococcus sp. strain WH 8103: effect of nitrogen source and availability on gene expression. Applied and Environmental Microbiology 69 (12), 7009-7018.

Bissinger, J.E., Montagnes, D.J.S., Sharples, J., Atkinson, D., 2008. Predicting marine phytoplankton maximum growth rates from temperature: Improving on the Eppley curve using quantile regression. Limnology and Oceanography 53 (2), 487-493.

Blanchot, J., Rodier, M., Le Bouteiller, A., 1992. Effect of El Niño Southern Oscillation events on the distribution and abundance of phytoplankton in the Western Pacific Tropical Ocean along 165 E. Journal of Plankton Research 14 (1), 137-156.

1054 Boss, E., Behrenfeld, M., 2010. In situ evaluation of the initiation of the North
1055 Atlantic phytoplankton bloom. Geophysical Research Letters 37, 5.
1056 Bower, A.S., von Appen, W.-J., 2008. Interannual Variability in the Pathways of the
1057 North Atlantic Current over the Mid-Atlantic Ridge and the Impact of Topography.
1058 Journal of Physical Oceanography 38 (1), 104-120.
1059 Braman, R.S., Hendrix, S.A., 1989. Nanogram nitrite and nitrate determination in
1060 environmental and biological materials by vanadium(iii) reduction with chemi-
1061 luminescence detection. Analytical Chemistry 61 (24), 2715-2718.
1062 Buck, K.R., Chavez, F.P., Campbell, L., 1996. Basin-wide distributions of living carbon
1063 components and the inverted trophic pyramid of the central gyre of the North
1064 Atlantic Ocean, summer 1993. Aquatic Microbial Ecology 10 (3), 283-298.
1065 Cabello, A.M., Latasa, M., Forn, I., G. Morán, X.A., Massana, R., 2016. Vertical
1066 distribution of major photosynthetic picoeukaryotic groups in stratified marine
1067 waters. Environmental Microbiology, n/a-n/a.
1068 Campbell, L., Liu, H., Nolla, H.A., Vaulot, D., 1997. Annual variability of phytoplankton
1069 and bacteria in the subtropical North Pacific Ocean at Station ALOHA during the
1070 1991–1994 ENSO event. Deep Sea Research Part I: Oceanographic Research Papers
1071 44 (2), 167-192.
1072 Carpenter, E.J., Harvey, H.R., Fry, B., Capone, D.G., 1997. Biogeochemical tracers of
1073 the marine cyanobacterium Trichodesmium. Deep Sea Research Part I:
1074 Oceanographic Research Papers 44 (1), 27-38.
1075 Casciotti, K., Sigman, D., Hastings, M.G., Böhlke, J., Hilkert, A., 2002. Measurement of
1076 the oxygen isotopic composition of nitrate in seawater and freshwater using the
1077 denitrifier method. Analytical Chemistry 74 (19), 4905-4912.
1078 Casciotti, K.L., 2009. Inverse kinetic isotope fractionation during bacterial nitrite
1079 oxidation. Geochimica Et Cosmochimica Acta 73 (7), 2061-2076.
1080 Casciotti, K.L., Sigman, D.M., Ward, B.B., 2003. Linking diversity and stable isotope
1081 fractionation in ammonia-oxidizing bacteria. Geomicrobiology Journal 20 (4), 335-
1082 353.
1083 Casey, J.R., Aucan, J.P., Goldberg, S.R., Lomas, M.W., 2013. Changes in partitioning of
1084 carbon amongst photosynthetic pico- and nano-plankton groups in the Sargasso Sea
1085 in response to changes in the North Atlantic Oscillation. Deep-Sea Research Part Ii-
1086 Topical Studies in Oceanography 93, 58-70.
1087 Casey, J.R., Lomas, M.W., Mandecki, J., Walker, D.E., 2007. Prochlorococcus
1088 contributes to new production in the Sargasso Sea deep chlorophyll maximum.
1089 Geophysical Research Letters 34 (10).
1090 Cavender-Bares, K.K., Karl, D.M., Chisholm, S.W., 2001. Nutrient gradients in the
1091 western North Atlantic Ocean: Relationship to microbial community structure and
1092 comparison to patterns in the Pacific Ocean. Deep Sea Research Part I:
1093 Oceanographic Research Papers 48 (11), 2373-2395.
1094 Cetinić, I., Perry, M.J., D'Asaro, E., Briggs, N., Poulton, N., Sieracki, M.E., Lee, C.M.,
1095 2015. A simple optical index shows spatial and temporal heterogeneity in
1096 phytoplankton community composition during the 2008 North Atlantic Bloom
1097 Experiment. Biogeosciences 12 (7), 2179-2194.

1098 Checkley, D.M., Miller, C.A., 1989. Nitrogen isotope fractionation by oceanic
1099 zooplankton. Deep Sea Research Part A. Oceanographic Research Papers 36 (10),
1100 1449-1456.
1101 Chisholm, S.W., 1992. Phytoplankton Size. In: Falkowski, P.G., Woodhead, A.D.,
1102 Vivirito, K. (Eds.), Primary Productivity and Biogeochemical Cycles in the Sea.
1103 Springer US, pp. 213-237.
1104 Collier, J.L., Brahamsha, B., Palenik, B., 1999. The marine cyanobacterium
1105 *Synechococcus* sp. WH7805 requires urease (urea amiohydrolase, EC 3.5. 1.5) to
1106 utilize urea as a nitrogen source: molecular-genetic and biochemical analysis of the
1107 enzyme. Microbiology 145 (2), 447-459.
1108 d'Ovidio, F., De Monte, S., Alvain, S., Dandonneau, Y., Lévy, M., 2010. Fluid dynamical
1109 niches of phytoplankton types. Proceedings of the National Academy of Sciences of
1110 the United States of America 107 (43), 18366-18370.
1111 Dandonneau, Y., Deschamps, P.-Y., Nicolas, J.-M., Loisel, H., Blanchot, J., Montel, Y.,
1112 Thieuleux, F., Bécu, G., 2004. Seasonal and interannual variability of ocean color and
1113 composition of phytoplankton communities in the North Atlantic, equatorial Pacific
1114 and South Pacific. Deep Sea Research Part II: Topical Studies in Oceanography 51
1115 (1–3), 303-318.
1116 de Boyer Montégut, C., Madec, G., Fischer, A.S., Lazar, A., Iudicone, D., 2004. Mixed
1117 layer depth over the global ocean: An examination of profile data and a profile-
1118 based climatology. Journal of Geophysical Research: Oceans 109 (C12), C12003.
1119 Deutsch, C., Sarmiento, J.L., Sigman, D.M., Gruber, N., Dunne, J.P., 2007. Spatial
1120 coupling of nitrogen inputs and losses in the ocean. Nature 445 (7124), 163-167.
1121 DiFiore, P.J., Sigman, D.M., Dunbar, R.B., 2009. Upper ocean nitrogen fluxes in the
1122 Polar Antarctic Zone: Constraints from the nitrogen and oxygen isotopes of nitrate.
1123 Geochemistry, Geophysics, Geosystems 10 (11).
1124 Duce, R., LaRoche, J., Altieri, K., Arrigo, K., Baker, A., Capone, D., Cornell, S., Dentener,
1125 F., Galloway, J., Ganeshram, R., 2008. Impacts of atmospheric anthropogenic
1126 nitrogen on the open ocean. Science 320 (5878), 893-897.
1127 Dufresne, A., Salanoubat, M., Partensky, F., Artiguenave, F., Axmann, I.M., Barbe, V.,
1128 Duprat, S., Galperin, M.Y., Koonin, E.V., Le Gall, F., 2003. Genome sequence of the
1129 cyanobacterium *Prochlorococcus* marinus SS120, a nearly minimal oxyphototrophic
1130 genome. Proceedings of the National Academy of Sciences 100 (17), 10020-10025.
1131 Dugdale, R.C., Goering, J.J., 1967. Uptake of new and regenerated forms of nitrogen in
1132 primary productivity. Limnology and Oceanography 12 (2), 196-206.
1133 DuRand, M.D., Olson, R.J., Chisholm, S.W., 2001. Phytoplankton population dynamics
1134 at the Bermuda Atlantic Time-series station in the Sargasso Sea. Deep-Sea Research
1135 Part Ii-Topical Studies in Oceanography 48 (8-9), 1983-2003.
1136 Eppley, R.W., 1972. Temperature and phytoplankton growth in sea. Fishery Bulletin
1137 70 (4), 1063-1085.
1138 Eppley, R.W., Peterson, B.J., 1979. Particulate organic-matter flux and planktonic
1139 new production in the deep ocean. Nature 282 (5740), 677-680.
1140 Fawcett, S.E., Lomas, M., Casey, J.R., Ward, B.B., Sigman, D.M., 2011. Assimilation of
1141 upwelled nitrate by small eukaryotes in the Sargasso Sea. Nature Geoscience 4 (10),
1142 717-722.

Fawcett, S.E., Lomas, M.W., Ward, B.B., Sigman, D.M., 2014. The counterintuitive effect of summer‐to‐fall mixed layer deepening on eukaryotic new production in the Sargasso Sea. Global Biogeochemical Cycles 28 (2), 86-102.
Fawcett, S.E., Ward, B.B., Lomas, M.W., Sigman, D.M., 2015. Vertical decoupling of nitrate assimilation and nitrification in the Sargasso Sea. Deep Sea Research Part I: Oceanographic Research Papers 103, 64-72.
Fuller, N.J., Marie, D., Partensky, F., Vaulot, D., Post, A.F., Scanlan, D.J., 2003. Clade-specific 16S ribosomal DNA oligonucleotides reveal the predominance of a single marine *Synechococcus* clade throughout a stratified water column in the Red Sea. Applied and Environmental Microbiology 69 (5), 2430-2443.
García-Ibáñez, M.I., Pardo, P.C., Carracedo, L.I., Mercier, H., Lherminier, P., Ríos, A.F., Pérez, F.F., 2015. Structure, transports and transformations of the water masses in the Atlantic Subpolar Gyre. Progress in Oceanography 135, 18-36.
Garçon, V.C., Oschlies, A., Doney, S.C., McGillicuddy, D., Waniek, J., 2001. The role of mesoscale variability on plankton dynamics in the North Atlantic. Deep Sea Research Part II: Topical Studies in Oceanography 48 (10), 2199-2226.
Gasol, J.M., Del Giorgio, P.A., 2000. Using flow cytometry for counting natural planktonic bacteria and understanding the structure of planktonic bacterial communities. Scientia Marina 64 (2), 197-224.
Glibert, P., Kana, T., Olson, R., Kirchman, D., Alberte, R., 1986. Clonal comparisons of growth and photosynthetic responses to nitrogen availability in marine *Synechococcus* spp. Journal of Experimental Marine Biology and Ecology 101 (1-2), 199-208.
Glover, H.E., Garside, C., Trees, C.C., 2007. Physiological responses of Sargasso Sea picoplankton to nanomolar nitrate perturbations. Journal of Plankton Research 29 (3), 263-274.
Glover, H.E., Prézelin, B.B., Campbell, L., Campbell, M., Garside, C., 1988. A nitrate-dependent *Synechococcus* bloom in surface Sargasso Sea water. Nature 331 (6152), 161-163.
Granger, J., Sigman, D.M., 2009. Removal of nitrite with sulfamic acid for nitrate N and O isotope analysis with the denitrifier method. Rapid Communications in Mass Spectrometry 23 (23), 3753-3762.
Grob, C., Hartmann, M., Zubkov, M.V., Scanlan, D.J., 2011. Invariable biomass-specific primary production of taxonomically discrete picoeukaryote groups across the Atlantic Ocean. Environmental Microbiology 13 (12), 3266-3274.
Gruber, N., Sarmiento, J.L., 1997. Global patterns of marine nitrogen fixation and denitrification. Global Biogeochemical Cycles 11 (2), 235-266.
Heywood, J.L., Zubkov, M.V., Tarran, G.A., Fuchs, B.M., Holligan, P.M., 2006. Prokaryoplankton standing stocks in oligotrophic gyre and equatorial provinces of the Atlantic Ocean: Evaluation of inter-annual variability. Deep Sea Research Part II: Topical Studies in Oceanography 53 (14–16), 1530-1547.
Hoch, M.P., Fogel, M.L., Kirchman, D.L., 1992. Isotope fractionation associated with ammonium uptake by a marine bacterium. Limnology and Oceanography 37 (7), 1447-1459.

1187 Holligan, P.M., Fernandez, E., Aiken, J., Balch, W.M., Boyd, P., Burkill, P.H., Finch, M.,
1188 Groom, S.B., Malin, G., Muller, K., Purdie, D.A., Robinson, C., Trees, C.C., Turner, S.M.,
1189 Vanderwal, P., 1993. A biogeochemical study of the coccolithophore, *Emiliania*
1190 *huxleyi*, in the North-Atlantic. Global Biogeochemical Cycles 7 (4), 879-900.
1191 Holm-Hansen, O., Riemann, B., 1978. Chlorophyll *a* Determination - Improvements
1192 in Methodology. Oikos 30, 438-447.
1193 Hooks, C.E., Bidigare, R.R., Keller, M.D., Guillard, R.R., 1988. Coccoid eukaryotic
1194 marine ultraplankters with four different hplc pigment signatures. Journal of
1195 Phycology 24 (4), 571-580.
1196 Hydes, D.J., Aoyama, M., Aminot, A., Bakker, K., Becker, S., Coverly, S., Daniel, A.,
1197 Dickson, A.G., Grosso, O., Kerouel, R., van Ooijen, J., Sato, K., Tanhua, T., Woodward,
1198 E.M.S., Zhang, J.Z., 2010. Determination of dissolved nutrients (N, P, Si) in seawater
1199 with high precision and inter-comparability using gas-segmented continuous flow
1200 analysers. The GO-SHIP Repeat Hyrography Manual: a collection of expert reports
1201 and guidelines.
1202 Irwin, A.J., Nelles, A.M., Finkel, Z.V., 2012. Phytoplankton niches estimated from field
1203 data. Limnology and Oceanography 57 (3), 787-797.
1204 Joint, I., Pomroy, A., Savidge, G., Boyd, P., 1993. Size-fractionated primary
1205 productivity in the northeast Atlantic in May–July 1989. Deep Sea Research Part II:
1206 Topical Studies in Oceanography 40 (1), 423-440.
1207 Jones, R., 1991. An improved fluorescence method for the determination of
1208 nanomolar concentrations of ammonium in natural waters. Limnology and
1209 Oceanography 36 (4), 814-819.
1210 Kana, T.M., Feiwel, N.L., Flynn, L.C., 1992. Nitrogen starvation in marine
1211 *Synechococcus* strains: clonal differences in phycobiliprotein breakdown and energy
1212 coupling. Marine Ecology-Progress Series 88, 75-75.
1213 Kirkham, A.R., Lepere, C., Jardillier, L.E., Not, F., Bouman, H., Mead, A., Scanlan, D.J.,
1214 2013. A global perspective on marine photosynthetic picoeukaryote community
1215 structure. ISME J 7 (5), 922-936.
1216 Knap, A., Jickells, T., 1986. Significance of atmospheric-derived fixed nitrogen on
1217 productivity of the Sargasso Sea. Nature 320, 158-160.
1218 Knapp, A.N., DiFiore, P.J., Deutsch, C., Sigman, D.M., Lipschultz, F., 2008. Nitrate
1219 isotopic composition between Bermuda and Puerto Rico: Implications for N2
1220 fixation in the Atlantic Ocean. Global Biogeochemical Cycles 22 (3).
1221 Knapp, A.N., Sigman, D.M., Lipschultz, F., 2005. N isotopic composition of dissolved
1222 organic nitrogen and nitrate at the Bermuda Atlantic Time‐series Study site. Global
1223 Biogeochemical Cycles 19 (1).
1224 Laney, S.R., Sosik, H.M., 2014. Phytoplankton assemblage structure in and around a
1225 massive under-ice bloom in the Chukchi Sea. Deep Sea Research Part II: Topical
1226 Studies in Oceanography 105 (0), 30-41.
1227 Laws, E.A., Letelier, R.M., Karl, D.M., 2014. Estimating the compensation irradiance
1228 in the ocean: The importance of accounting for non-photosynthetic uptake of
1229 inorganic carbon. Deep Sea Research Part I: Oceanographic Research Papers 93 (0),
1230 35-40.

1231 Legendre, L., Gosselin, M., 1997. Estimation of N or C uptake rates by phytoplankton
1232 using N-15 or C-13: Revisiting the usual computation formulae. Journal of Plankton
1233 Research 19 (2), 263-271.
1234 Letelier, R.M., Karl, D.M., Abbott, M.R., Bidigare, R.R., 2004. Light driven seasonal
1235 patterns of chlorophyll and nitrate in the lower euphotic zone of the North Pacific
1236 Subtropical Gyr. Limnology and Oceanography 49 (2), 508-519.
1237 Li, W.K., 1994. Primary production of prochlorophytes, cyanobacteria, and
1238 eucaryotic ultraphytoplankton: measurements from flow cytometric sorting.
1239 Limnology and Oceanography 39 (1), 169-175.
1240 Li, W.K.W., 1995. Composition of ultraphytoplankton in the central North Atlantic.
1241 Marine Ecology Progress Series 122, 1-8.
1242 Li, W.K.W., 1997. Cytometric diversity in marine ultraphytoplankton. Limnology and
1243 Oceanography 42 (5), 874-880.
1244 Li, W.K.W., 2002. Macroecological patterns of phytoplankton in the northwestern
1245 North Atlantic Ocean. Nature 419 (6903), 154-157.
1246 Li, W.K.W., Harrison, W.G., 2001. Chlorophyll, bacteria and picophytoplankton in
1247 ecological provinces of the North Atlantic. Deep Sea Research Part II: Topical Studies
1248 in Oceanography 48 (10), 2271-2293.
1249 Lindell, D., Padan, E., Post, A.F., 1998. Regulation of ntcA expression and nitrite
1250 uptake in the marine Synechococcus sp. strain WH 7803. Journal of Bacteriology 180
1251 (7), 1878-1886.
1252 Liu, K.-K., Kao, S.-J., Chiang, K.-P., Gong, G.-C., Chang, J., Cheng, J.-S., Lan, C.-Y., 2013.
1253 Concentration dependent nitrogen isotope fractionation during ammonium uptake
1254 by phytoplankton under an algal bloom condition in the Danshuei estuary, northern
1255 Taiwan. Marine Chemistry 157, 242-252.
1256 Lochte, K., Ducklow, H.W., Fasham, M.J.R., Stienen, C., 1993. Plankton succession and
1257 carbon cycling at 47°N-20°W during the JGOFS North-Atlantic bloom experiment.
1258 Deep-Sea Research Part Ii-Topical Studies in Oceanography 40 (1-2), 91-114.
1259 Lomas, M.W., Bonachela, J.A., Levin, S.A., Martiny, A.C., 2014. Impact of ocean
1260 phytoplankton diversity on phosphate uptake. Proceedings of the National Academy
1261 of Sciences 111 (49), 17540-17545.
1262 Lomas, M.W., Lipschultz, F., 2006. Forming the primary nitrite maximum: Nitrifiers
1263 or phytoplankton? Limnology and Oceanography 51 (5), 2453-2467.
1264 Lomas, M.W., Moran, S.B., 2011. Evidence for aggregation and export of
1265 cyanobacteria and nano-eukaryotes from the Sargasso Sea euphotic zone.
1266 Biogeosciences 8 (1), 203-216.
1267 Longhurst, A., 2007. Ecological Geography of the Sea. Academic Press, London.
1268 Macko, S.A., Estep, M.L.F., Engel, M.H., Hare, P., 1986. Kinetic fractionation of stable
1269 nitrogen isotopes during amino acid transamination. Geochimica Et Cosmochimica
1270 Acta 50 (10), 2143-2146.
1271 Marañón, E., Cermeno, P., Latasa, M., Tadonléké, R.D., 2012. Temperature, resources,
1272 and phytoplankton size structure in the ocean. Limnology and Oceanography 57 (5),
1273 1266.
1274 Marañon, E., Holligan, P.M., Barciela, R., González, N., Mouriño, B., Pazó, M.J., Varela,
1275 M., 2001. Patterns of phytoplankton size structure and productivity in contrasting
1276 open-ocean environments. Marine Ecology Progress Series 216, 43-56.

1277 Marconi, D., Weigand, M.A., Rafter, P.A., McIlvin, M.R., Forbes, M., Casciotti, K.L.,
1278 Sigman, D.M., 2015. Nitrate isotope distributions on the US GEOTRACES North
1279 Atlantic cross-basin section: Signals of polar nitrate sources and low latitude
1280 nitrogen cycling. Marine Chemistry 177, 143-156.
1281 Marie, D., Partensky, F., Jacquet, S., Vaulot, D., 1997. Enumeration and cell cycle
1282 analysis of natural populations of marine picoplankton by flow cytometry using the
1283 nucleic acid stain SYBR Green I. Applied and Environmental Microbiology 63 (1),
1284 186-193.
1285 Mariotti, A., Germon, J., Hubert, P., Kaiser, P., Letolle, R., Tardieux, A., Tardieux, P.,
1286 1981. Experimental determination of nitrogen kinetic isotope fractionation: some
1287 principles; illustration for the denitrification and nitrification processes. Plant and
1288 soil 62 (3), 413-430.
1289 Marra, J.F., Lance, V.P., Vaillancourt, R.D., Hargreaves, B.R., 2014. Resolving the
1290 ocean's euphotic zone. Deep Sea Research Part I: Oceanographic Research Papers 83
1291 (0), 45-50.
1292 Martiny, A.C., Kathuria, S., Berube, P.M., 2009. Widespread metabolic potential for
1293 nitrite and nitrate assimilation among Prochlorococcus ecotypes. Proceedings of the
1294 National Academy of Sciences 106 (26), 10787-10792.
1295 McIlvin, M.R., Casciotti, K.L., 2011. Technical updates to the bacterial method for
1296 nitrate isotopic analyses. Analytical Chemistry 83 (5), 1850-1856.
1297 Michaels, A.F., Siegel, D.A., Johnson, R.J., Knap, A.H., Galloway, J.N., 1993. Episodic
1298 inputs of atmospheric nitrogen to the Sargasso Sea: Contributions to new
1299 production and phytoplankton blooms. Global Biogeochemical Cycles 7, 339-351.
1300 Minagawa, M., Wada, E., 1986. Nitrogen isotope ratios of red tide organisms in the
1301 East China Sea: a characterization of biological nitrogen fixation. Marine Chemistry
1302 19 (3), 245-259.
1303 Möbius, J., 2013. Isotope fractionation during nitrogen remineralization
1304 (ammonification): Implications for nitrogen isotope biogeochemistry. Geochimica Et
1305 Cosmochimica Acta 105, 422-432.
1306 Montoya, J.P., Carpenter, E.J., Capone, D.G., 2002. Nitrogen fixation and nitrogen
1307 isotope abundances in zooplankton of the oligotrophic North Atlantic. Limnology
1308 and Oceanography 47 (6), 1617-1628.
1309 Moore, C.M., Mills, M.M., Arrigo, K.R., Berman-Frank, I., Bopp, L., Boyd, P.W.,
1310 Galbraith, E.D., Geider, R.J., Guieu, C., Jaccard, S.L., Jickells, T.D., La Roche, J., Lenton,
1311 T.M., Mahowald, N.M., Maranon, E., Marinov, I., Moore, J.K., Nakatsuka, T., Oschlies,
1312 A., Saito, M.A., Thingstad, T.F., Tsuda, A., Ulloa, O., 2013. Processes and patterns of
1313 oceanic nutrient limitation. Nature Geosci 6 (9), 701-710.
1314 Moore, C.M., Mills, M.M., Langlois, R., Milne, A., Achterberg, E.P., LaRoche, J., Geider,
1315 R.J., 2008. Relative influence of nitrogen and phosphorous availability on
1316 phytoplankton physiology and productivity in the oligotrophic sub-tropical North
1317 Atlantic Ocean. Limnology and Oceanography 53 (1), 291-305.
1318 Moore, L.R., Coe, A., Zinser, E.R., Saito, M.A., Sullivan, M.B., Lindell, D., Frois-Moniz, K.,
1319 Waterbury, J., Chisholm, S.W., 2007. Culturing the marine cyanobacterium
1320 *Prochlorococcus*. Limnol. Oceanogr. Methods 5, 353-362.

1321 Moore, L.R., Post, A.F., Rocap, G., Chisholm, S.W., 2002. Utilization of different
1322 nitrogen sources by the marine cyanobacteria *Prochlorococcus* and *Synechococcus*.
1323 Limnology and Oceanography 47 (4), 989-996.
1324 Morel, A., Berthon, J.F., 1989. Surface pigments, algal biomass profiles, and potential
1325 production of the euphotic layer - relationships reinvestigated in view of remote-
1326 sensing applications. Limnology and Oceanography 34 (8), 1545-1562.
1327 Morel, A., Maritorena, S., 2001. Bio-optical properties of oceanic waters: A
1328 reappraisal. Journal of Geophysical Research: Oceans 106 (C4), 7163-7180.
1329 Nielsdóttir, M.C., Moore, C.M., Sanders, R., Hinz, D.J., Achterberg, E.P., 2009. Iron
1330 limitation of the postbloom phytoplankton communities in the Iceland Basin. Global
1331 Biogeochemical Cycles 23 (3), n/a-n/a.
1332 Olson, R.J., Chisholm, S.W., Zettler, E.R., Altabet, M.A., Dusenberry, J.A., 1990. Spatial
1333 and temporal distributions of prochlorophyte picoplankton in the North Atlantic
1334 Ocean. Deep Sea Research Part A. Oceanographic Research Papers 37 (6), 1033-
1335 1051.
1336 Olson, R.J., Zettler, E.R., Anderson, O.K., 1989. Discrimination of eukaryotic
1337 phytoplankton cell types from light scatter and autofluorescence properties
1338 measured by flow cytometry. Cytometry 10 (5), 636-643.
1339 Oschlies, A., 2002. Nutrient supply to the surface waters of the North Atlantic: A
1340 model study. Journal of Geophysical Research: Oceans 107 (C5), 14-11-14-13.
1341 Paerl, H.W., 1991. Ecophysiological and trophic implications of light-stimulated
1342 amino acid utilization in marine picoplankton. Applied and Environmental
1343 Microbiology 57 (2), 473-479.
1344 Painter, S.C., Patey, M.D., Tarran, G.A., Torres-Valdès, S., 2014. Picoeukaryote
1345 distribution in relation to nitrate uptake in the oceanic nitracline. Aquatic Microbial
1346 Ecology 72 (3), 195-213.
1347 Partensky, F., Blanchot, J., Lantoine, F., Neveux, J., Marie, D., 1996. Vertical structure
1348 of picophytoplankton at different trophic sites of the tropical northeastern Atlantic
1349 Ocean. Deep Sea Research Part I: Oceanographic Research Papers 43 (8), 1191-
1350 1213.
1351 Partensky, F., Blanchot, J., Vaulot, D., 1999a. Differential distribution and ecology of
1352 *Prochlorococcus* and *Synechococcus* in oceanic waters: a review. Bulletin Institut
1353 Oceanographique Monaco numero special, 457-476.
1354 Partensky, F., Hess, W.R., Vaulot, D., 1999b. *Prochlorococcus*, a marine
1355 photosynthetic prokaryote of global significance. Microbiology and Molecular
1356 Biology Reviews 63 (1), 106-127.
1357 Pennock, J.R., Velinsky, D.J., Ludlam, J.M., Sharp, J.H., Fogel, M.L., 1996. Isotopic
1358 fractionation of ammonium and nitrate during uptake by *Skeletonema costatum*:
1359 Implications for δ15N dynamics under bloom conditions. Limnology and
1360 Oceanography 41 (3), 451-459.
1361 Pomeroy, L.R., 1974. Oceans food web, a changing paradigm. Bioscience 24 (9), 499-
1362 504.
1363 Poulton, A.J., Charalampopoulou, A., Young, J.R., Tarran, G.A., Lucas, M.I., Quartly,
1364 G.D., 2010. Coccolithophore dynamics in non-bloom conditions during late summer
1365 in the central Iceland Basin (July-August 2007). Limnology and Oceanography 55
1366 (4), 1601-1613.

1367 Qi, H., Coplen, T.B., Geilmann, H., Brand, W.A., Böhlke, J., 2003. Two new organic
1368 reference materials for δ13C and δ15N measurements and a new value for the δ13C
1369 of NBS 22 oil. Rapid Communications in Mass Spectrometry 17 (22), 2483-2487.
1370 Raimbault, P., Rodier, M., Taupier-Letage, I., 1988. Size fraction of phytoplankton in
1371 the Ligurian Sea and the Algerian Basin (Mediterranean Sea): Size distribution
1372 versus total concentration. Marine Microbial Food Webs 3 (1), 1-7.
1373 Reygondeau, G., Longhurst, A., Martinez, E., Beaugrand, G., Antoine, D., Maury, O.,
1374 2013. Dynamic biogeochemical provinces in the global ocean. Global Biogeochemical
1375 Cycles 27 (4), 1046-1058.
1376 Rodríguez, J., Blanco, J.M., Jiménez-Gómez, F., Echevarría, F., Gil, J., Rodríguez, V.,
1377 Ruiz, J., Bautista, B., Guerrero, F., 1998. Patterns in the size structure of the
1378 phytoplankton community in the deep fluorescence maximum of the Alboran Sea
1379 (southwestern mediterranean). Deep Sea Research Part I: Oceanographic Research
1380 Papers 45 (10), 1577-1593.
1381 Rynearson, T.A., Richardson, K., Lampitt, R.S., Sieracki, M.E., Poulton, A.J.,
1382 Lyngsgaard, M.M., Perry, M.J., 2013. Major contribution of diatom resting spores to
1383 vertical flux in the sub-polar North Atlantic. Deep Sea Research Part I:
1384 Oceanographic Research Papers 82, 60-71.
1385 Saito, M.A., McIlvin, M.R., Moran, D.M., Goepfert, T.J., DiTullio, G.R., Post, A.F.,
1386 Lamborg, C.H., 2014. Multiple nutrient stresses at intersecting Pacific Ocean biomes
1387 detected by protein biomarkers. Science 345 (6201), 1173-1177.
1388 Sambrotto, R.N., Martin, J.H., Broenkow, W.W., Carlson, C., Fitzwater, S.E., 1993.
1389 Nitrate utilization in surface waters of the Iceland Basin during spring and summer
1390 of 1989. Deep Sea Research Part II: Topical Studies in Oceanography 40 (1), 441-
1391 457.
1392 Scanlan, D.J., 2003. Physiological diversity and niche adaptation in marine
1393 *Synechococcus*. Advances in microbial physiology 47, 1-64.
1394 Scanlan, D.J., Post, A.F., 2008. Aspects of marine cyanobacterial nitrogen physiology
1395 and connection to the nitrogen cycle. In: Capone, D.G., Bronk, D.A., Mulholland, M.R.,
1396 Carpenter, E.J. (Eds.), Nitrogen in the marine environment. Academic Press, San
1397 Diego, CA, p. 1073–1195.
1398 Schlitzer, R., 2015. Ocean Data View, http://odv.awi.de/. http://odv.awi.de/.
1399 Sieburth, J.M., Smetacek, V., Lenz, J., 1978. Pelagic ecosystem structure:
1400 Heterotrophic compartments of the plankton and their relationship to plankton size
1401 fractions 1. Limnology and Oceanography 23 (6), 1256-1263.
1402 Sieracki, M.E., Verity, P.G., Stoecker, D.K., 1993. Plankton community response to
1403 sequential silicate and nitrate depletion during the 1989 North Atlantic spring
1404 bloom. Deep-Sea Research Part Ii-Topical Studies in Oceanography 40 (1-2), 213-
1405 225.
1406 Sigman, D., Altabet, M., McCorkle, D., Francois, R., Fischer, G., 1999. The δ15N of
1407 nitrate in the Southern Ocean: consumption of nitrate in surface waters. Global
1408 Biogeochemical Cycles 13 (4), 1149-1166.
1409 Sigman, D., Altabet, M., McCorkle, D., Francois, R., Fischer, G., 2000. The δ15N of
1410 nitrate in the Southern Ocean: nitrogen cycling and circulation in the ocean interior.
1411 Journal of Geophysical Research: Oceans 105 (C8), 19599-19614.

1412 Sigman, D., Casciotti, K., Andreani, M., Barford, C., Galanter, M., Böhlke, J., 2001. A
1413 bacterial method for the nitrogen isotopic analysis of nitrate in seawater and
1414 freshwater. Analytical Chemistry 73 (17), 4145-4153.
1415 Sigman, D.M., Granger, J., DiFiore, P.J., Lehmann, M.M., Ho, R., Cane, G., van Geen, A.,
1416 2005. Coupled nitrogen and oxygen isotope measurements of nitrate along the
1417 eastern North Pacific margin. Global Biogeochemical Cycles 19 (4).
1418 Silfer, J., Engel, M., Macko, S., 1992. Kinetic fractionation of stable carbon and
1419 nitrogen isotopes during peptide bond hydrolysis: experimental evidence and
1420 geochemical implications. Chemical Geology: Isotope Geoscience Section 101 (3-4),
1421 211-221.
1422 Smart, S.M., Fawcett, S.E., Thomalla, S.J., Weigand, M.A., Reason, C.J., Sigman, D.M.,
1423 2015. Isotopic evidence for nitrification in the Antarctic winter mixed layer. Global
1424 Biogeochemical Cycles 29 (4), 427-445.
1425 Straub, M., Tremblay, M., Sigman, D., Studer, A., Ren, H., Toggweiler, J., Haug, G.,
1426 2013. Nutrient conditions in the subpolar North Atlantic during the last glacial
1427 period reconstructed from foraminifera ‐ bound nitrogen isotopes.
1428 Paleoceanography 28 (1), 79-90.
1429 Talley, L.D., 2011. Descriptive physical oceanography: an introduction. Academic
1430 press.
1431 Tarran, G.A., Heywood, J.L., Zubkov, M.V., 2006. Latitudinal changes in the standing
1432 stocks of nano- and picoeukaryotic phytoplankton in the Atlantic Ocean. Deep Sea
1433 Research Part II: Topical Studies in Oceanography 53 (14–16), 1516-1529.
1434 Tarran, G.A., Zubkov, M.V., Sleigh, M.A., Burkill, P.H., Yallop, M., 2001. Microbial
1435 community structure and standing stocks in the NE Atlantic in June and July of 1996.
1436 Deep-Sea Research Part Ii-Topical Studies in Oceanography 48 (4-5), 963-985.
1437 Treibergs, L.A., Fawcett, S.E., Lomas, M.W., Sigman, D.M., 2014. Nitrogen isotopic
1438 response of prokaryotic and eukaryotic phytoplankton to nitrate availability in
1439 Sargasso Sea surface waters. Limnol. Oceanogr 59 (3), 972-985.
1440 Troupin, C., Barth, A., Sirjacobs, D., Ouberdous, M., Brankart, J.-M., Brasseur, P.,
1441 Rixen, M., Alvera-Azcarate, A., Belounis, M., Capet, A., Lenartz, F., Toussaint, M.-E.,
1442 Beckers, J.-M., 2012. Generation of analysis and consistent error fields using the
1443 Data Interpolating Variational Analysis (Diva). Ocean Modelling 52-53, 90-101.
1444 Vaulot, D., Eikrem, W., Viprey, M., Moreau, H., 2008. The diversity of small eukaryotic
1445 phytoplankton (≤ 3 μm) in marine ecosystems. FEMS microbiology reviews 32 (5),
1446 795-820.
1447 Verity, P.G., Robertson, C.Y., Tronzo, C.R., Andrews, M.G., Nelson, J.R., Sieracki, M.E.,
1448 1992. Relationships between cell-volume and the carbon and nitrogen-content of
1449 marine photosynthetic nanoplankton. Limnology and Oceanography 37 (7), 1434-
1450 1446.
1451 Wada, E., Hattori, A., 1978. Nitrogen isotope effects in the assimilation of inorganic
1452 nitrogenous compounds. Geo Microbiology 7 (7), 85-101.
1453 Wankel, S.D., Kendall, C., Pennington, J.T., Chavez, F.P., Paytan, A., 2007. Nitrification
1454 in the euphotic zone as evidenced by nitrate dual isotopic composition:
1455 Observations from Monterey Bay, California. Global Biogeochemical Cycles 21 (2).

1456 Weigand, M.A., Foriel, J., Barnett, B., Oleynik, S., Sigman, D.M., 2016. Updates to
1457 instrumentation and protocols for isotopic analysis of nitrate by the denitrifier
1458 method. Rapid Communications in Mass Spectrometry 30 (12), 1365-1383.
1459 Woodward, E.M.S., Rees, A.P., 2001. Nutrient distributions in an anticyclonic eddy in
1460 the North East Atlantic Ocean, with reference to nanomolar ammonium
1461 concentrations. Deep Sea Research Part II: Topical Studies in Oceanography 48 (4-
1462 5), 775-794.
1463 Wyman, M., Gregory, R., Carr, N., 1985. Novel role for phycoerythrin in a marine
1464 cyanobacterium, Synechococcus strain DC2. Science 230 (4727), 818-820.
1465 Yool, A., Martin, A.P., Fernández, C., Clark, D.R., 2007. The significance of nitrification
1466 for oceanic new production. Nature 447 (7147), 999-1002.
1467 Zinser, E.R., Coe, A., Johnson, Z.I., Martiny, A.C., Fuller, N.J., Scanlan, D.J., Chisholm,
1468 S.W., 2006. *Prochlorococcus* Ecotype Abundances in the North Atlantic Ocean As
1469 Revealed by an Improved Quantitative PCR Method. Applied and Environmental
1470 Microbiology 72 (1), 723-732.
1471 Zubkov, M.V., Fuchs, B.M., Tarran, G.A., Burkill, P.H., Amann, R., 2003. High rate of
1472 uptake of organic nitrogen compounds by *Prochlorococcus* cyanobacteria as a key to
1473 their dominance in oligotrophic oceanic waters. Applied and Environmental
1474 Microbiology 69 (2), 1299-1304.
1475 Zubkov, M.V., Sleigh, M.A., Tarran, G.A., Burkill, P.H., Leakey, R.J.G., 1998.
1476 Picoplanktonic community structure on an Atlantic transect from 50°N to 50°S.
1477 Deep Sea Research Part I: Oceanographic Research Papers 45 (8), 1339-1355.
1478 Zubkov, M.V., Tarran, G.A., 2005. Amino acid uptake of Prochlorococcus spp. in
1479 surface waters across the South Atlantic Subtropical Front. Aquatic Microbial
1480 Ecology 40 (3), 241-249.
1481 Zwirglmaier, K., Jardillier, L., Ostrowski, M., Mazard, S., Garczarek, L., Vaulot, D., Not,
1482 F., Massana, R., Ulloa, O., Scanlan, D.J., 2008. Global phylogeography of marine
1483 *Synechococcus* and *Prochlorococcus* reveals a distinct partitioning of lineages among
1484 oceanic biomes. Environmental Microbiology 10 (1), 147-161.
1485

1486

Figure 1. Bathymetric map of stations in the southwest (black symbols), shelf (grey symbol) and northeast (white symbols) section of the transect.

Figure 2. Section plots of (A) temperature (colour shaded), (B) salinity (colour shaded), and (C) nitrate concentration (colour shaded and contour lines) along the transect. Contour lines in A and B represent the potential density anomaly (sigma-theta). Dotted profiles are associated with station numbers listed at the top of the figure. The higher spatial frequency of the surface values is the result of 6-hourly underway sampling. The thick grey dashed line indicates the depth of the nitracline.

Figure 3. Depth section plots of (A) suspended particulate organic nitrogen and (B) suspended particulate organic carbon concentration. The thick grey dashed line indicates the depth of the nitracline. Transect station numbers are designated at the top of the figure.

Figure 4. Depth section plots of (A) the N isotopic composition of suspended particulate organic nitrogen (δ^{15}N-PN) with contour lines indicating PN concentration (μmol l^{-1}), and (B) the N isotopic composition of nitrate (δ^{15}N-NO_3^-) with NO_3^- concentration contour lines (μmol l^{-1}). Station numbers are listed at the top of the figure. The thick grey dashed line indicates the depth of the nitracline and the grey circles indicate samples where the PN or NO_3^- concentration was too low for its isotopic composition to be measured.

Figure 5. Depth section plots of (A) chlorophyll *a* and (B) combined pico- and nanophytoplankton carbon biomass concentration along the transect course. Dotted profile samples are associated with station numbers listed at the top of the figure. The thick grey dashed line indicates the depth of the nitracline and the thick white dashed line represents the light compensation depth (Z_{lc} at 0.17 mol PAR quanta m^{-2} day^{-1}).

Figure 6. Depth-integrated chlorophyll *a* (ΣChla) in each size fraction (<2 μm, 2-20 μm and >20 μm) above the light compensation depth (Z_{lc}, see Table 1) as a percentage of the total integrated Chla measured at each station (solid black line).

Figure 7. Depth section plots of the carbon biomass concentration of (A) *Prochlorococcus*, (B) *Synechococcus*, (C) picoeukaryotes, and (D) nanophytoplankton as enumerated by flow cytometry across the transect course. Dotted profile samples are associated with the station numbers listed at the top of the figure. The thick grey dashed line indicates the depth of the nitracline. Note the difference in colour bar scale for each phytoplankton group.

Figure 8. Depth section plots of the proportion of biomass represented by (A) *Prochlorococcus*, (B) *Synechococcus*, (C) picoeukaryotes, and (D) nanoeukaryotes as determined by flow cytometry. The thick grey dashed line indicates the depth of the nitracline and the thick white dashed line represents the light compensation depth (Z_{lc} at 0.17 mol PAR quanta m^{-2} day^{-1}). Dotted profile samples are associated with the station numbers listed at the top of the figure. Samples with a potentially unrepresentative population estimates (<250 nanophytoplankton cells counted) are greyed-out. Note that the different phytoplankton groups are plotted using different colour scales selected to emphasise their distribution patterns.

Figure 9. Depth section plots of (A) inorganic carbon fixation rate (transport rate; ρDIC) and (B) inorganic carbon fixation rate normalised to flow cytometry-derived phytoplankton biomass (specific rate; *V*DIC). The thick grey dashed line indicates the depth of the nitracline. Dotted profile samples are associated with the station numbers listed at the top of the figure.

Figure 10. The distribution of relative nanoeukaryote (A) and picocyanobacteria (B) depth-integrated carbon biomass contribution as a function of the upper ocean mass-weighted $\delta^{15}N$ of PN minus the $\delta^{15}N$ of the subsurface nitrate source ($\delta^{15}N_{PN}$ -

$\delta^{15}N_{NO3\text{-}source}$), as a proxy for nitrate utilisation. Phytoplankton carbon biomass and δ^{15}N-PN data from each station (excluding station 7, see Methods section) are from the surface to the nitracline depth or the MLD, whichever was deepest. Station symbols as in Figure 1.

Figure 1. Bathymetric map of stations in the southwest (black symbols), shelf (grey symbol) and northeast (white symbols) section of the transect. The stations belong to the biogeographical provinces (*sensu* Longhurst 2007) of the Gulf Stream (GFST, circles), Northwest Atlantic shelves (NWCS, star), North Atlantic Drift (NADR, diamonds) and Atlantic subarctic (SARC, square).

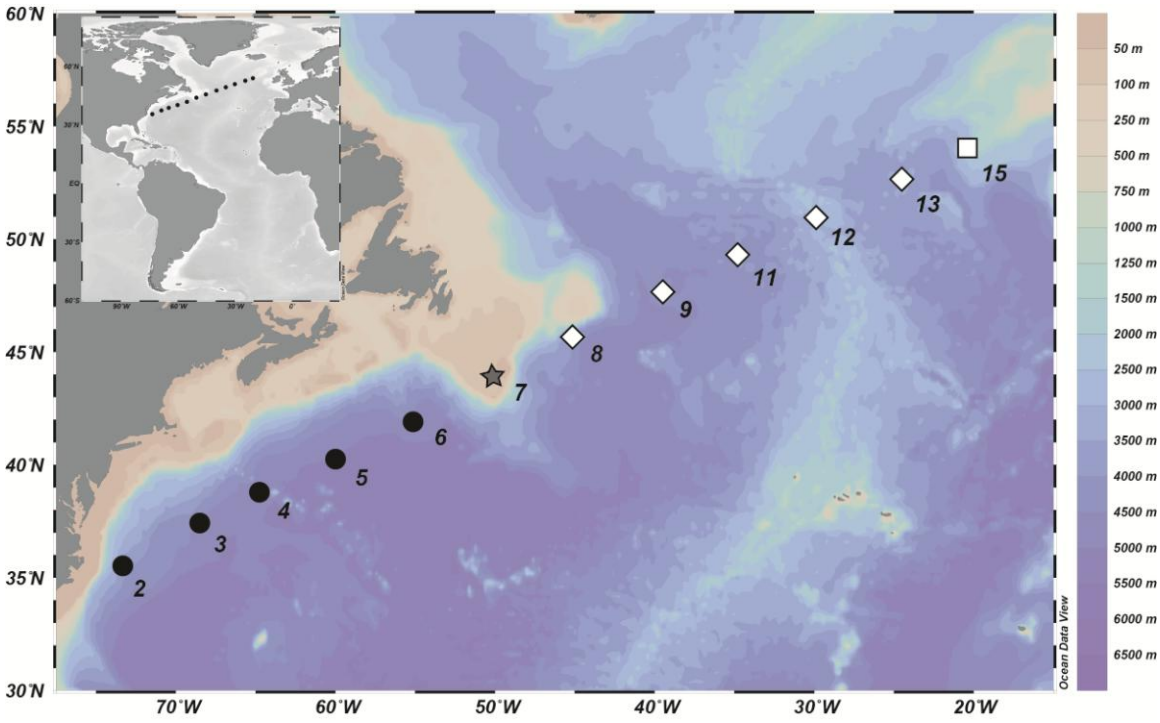

Figure 2. Section plots of (A) temperature (colour shaded), (B) salinity (colour shaded), and (C) nitrate concentration (colour shaded) along the transect. Contour lines represent the potential density anomaly (sigma-theta). Dotted profiles are associated with station numbers listed at the top of the figure. The higher spatial frequency of the surface values is the result of 6-hourly underway sampling. The thick grey dashed line indicates the depth of the nitracline ($[NO_3^-]$ = 300 nmol l^{-1}).

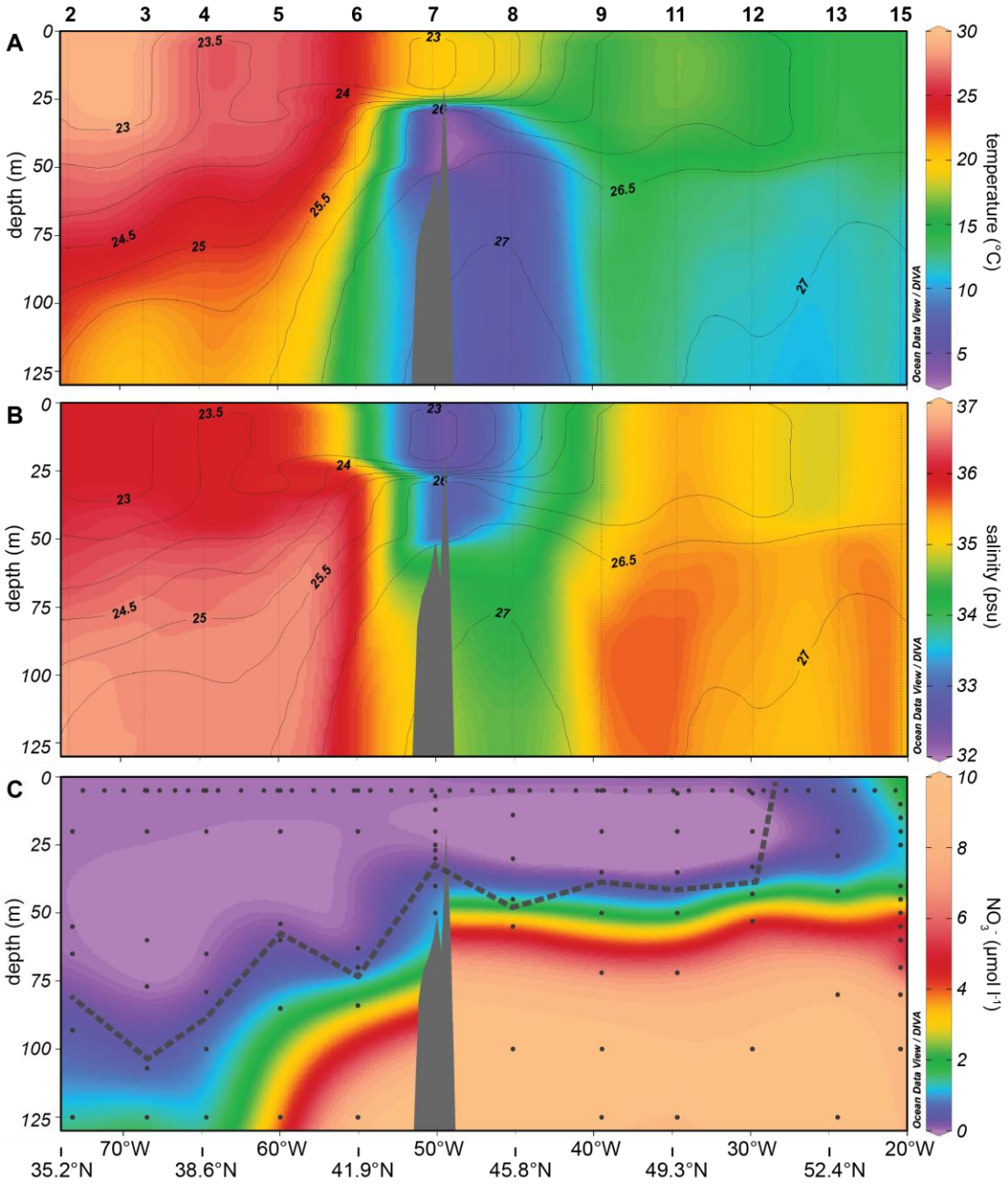

Figure 3. Depth section plots of (A) suspended particulate organic nitrogen and (B) suspended particulate organic carbon concentration. The thick black dashed line indicates the depth of the nitracline ([NO_3^-] = 300 nmol l^{-1}). Transect station numbers are designated at the top of the figure.

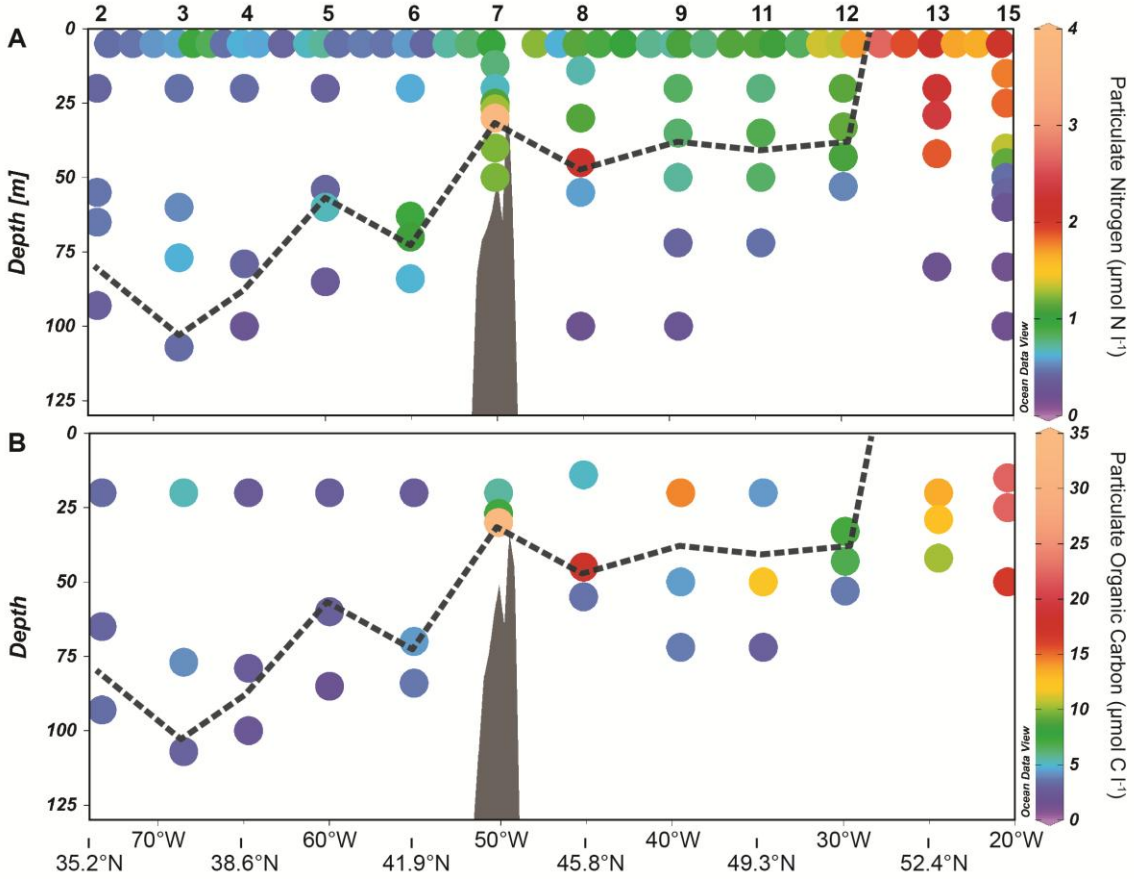

Figure 4. Depth section plots of (A) the N isotopic composition of suspended particulate organic nitrogen (δ^{15}N PN) with contour lines indicating PN concentration (µmol l^{-1}), and (B) the N isotopic composition of nitrate (δ^{15}N NO_3^-) with NO_3^- concentration contour lines (µmol l^{-1}). Station numbers are listed at the top of the figure. The thick dashed black line indicates the depth of the nitracline ([NO_3^-] = 300 nmol l^{-1}) and the grey circles indicate samples where the PN or NO_3^- concentration was too low for its isotopic composition to be measured.

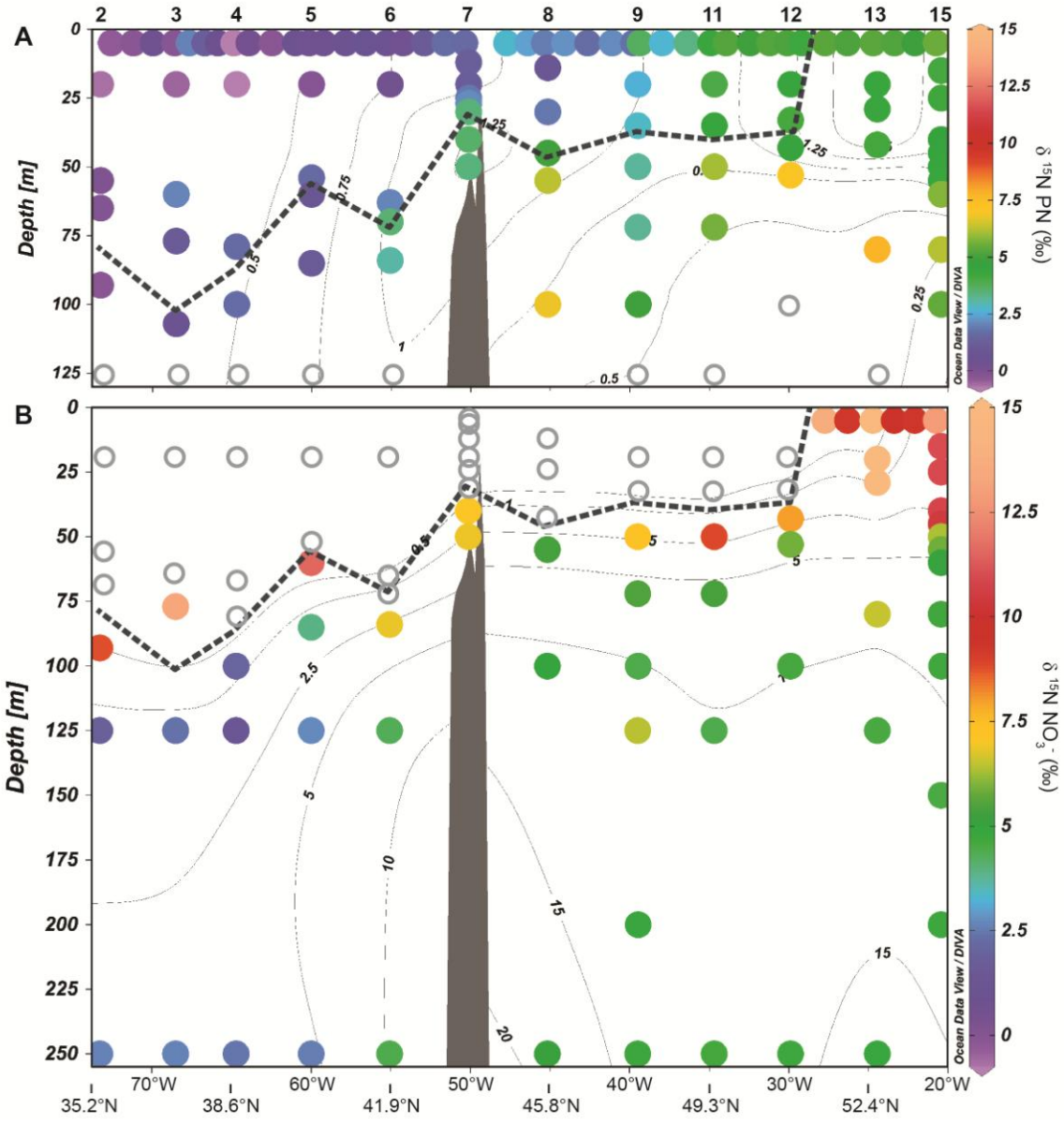

Figure 5. The distribution of relative nanoeukaryote (A) and picocyanobacteria (B) depth-integrated carbon biomass contribution as a function of the upper ocean mass-weighted $\delta^{15}N$ of PN minus the $\delta^{15}N$ of the subsurface nitrate source ($\delta^{15}N_{PN}$ - $\delta^{15}N_{NO3\text{-}source}$), as a proxy for nitrate utilisation. Phytoplankton carbon biomass and PN $\delta^{15}N$ data from each station (excluding station 7, see Methods section) are from the surface to the nitracline depth or the MLD, whichever was deepest. Station symbols as in Figure 1.

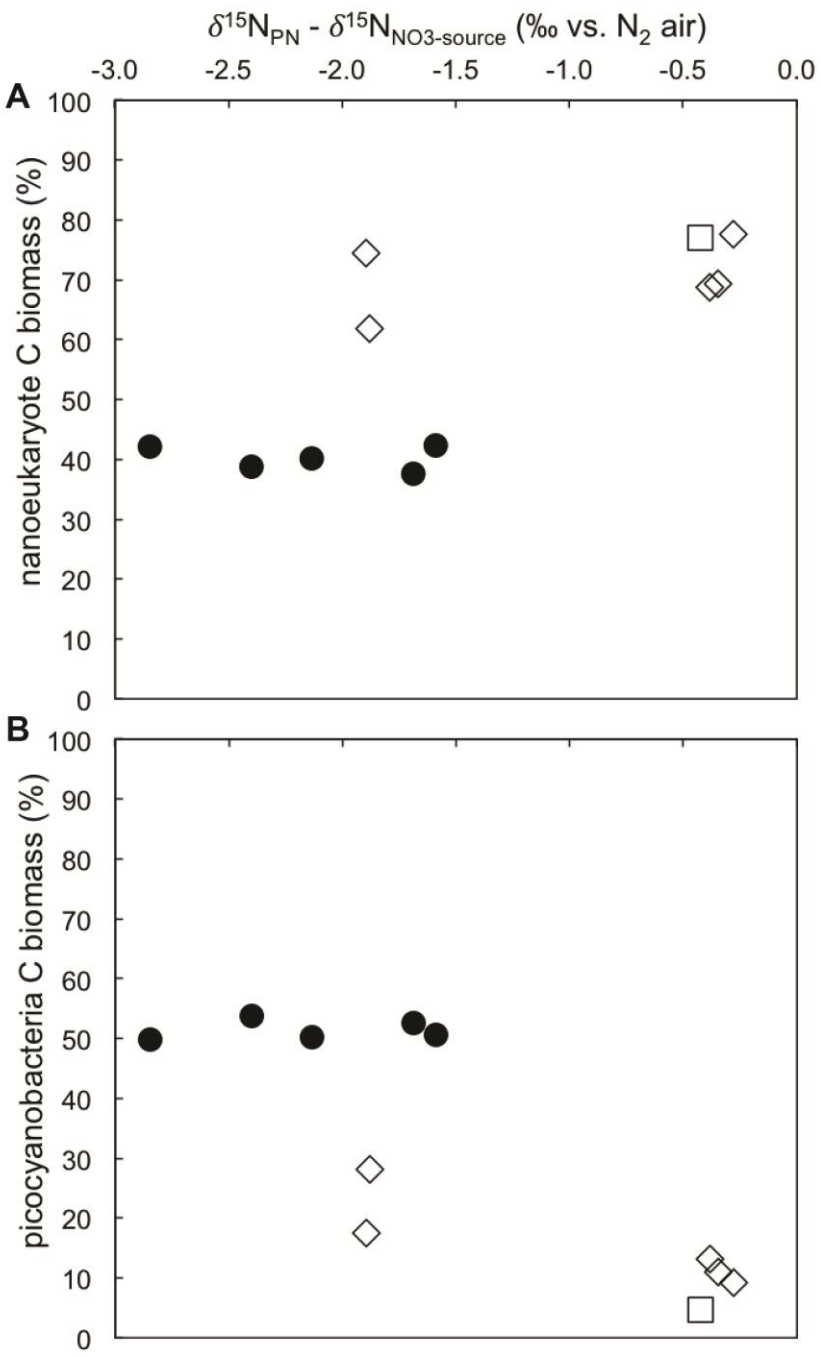
δ15NPN - δ15NNO3-source (‰ vs. N2 air)
-3.0
-2.5
-2.0
-1.5
-1.0
-0.5
0.0
A
nanoeukaryote C biomass (%)
B
picocyanobacteria C biomass (%)
0
10
20
30
40
50
60
70
80
90
100

Figure 6. Depth section plots of (A) chlorophyll *a* and (B) pico- and nanophytoplankton carbon biomass concentration along the transect course. Dotted profile samples are associated with station numbers listed at the top of the figure. The thick grey dashed line indicates the depth of the nitracline ($[NO_3^-]$ = 300 nmol l^{-1}) and the thick white dashed line represents the light compensation depth (Z_{Ic} at 0.17 mol PAR quanta m^{-2} day^{-1}).

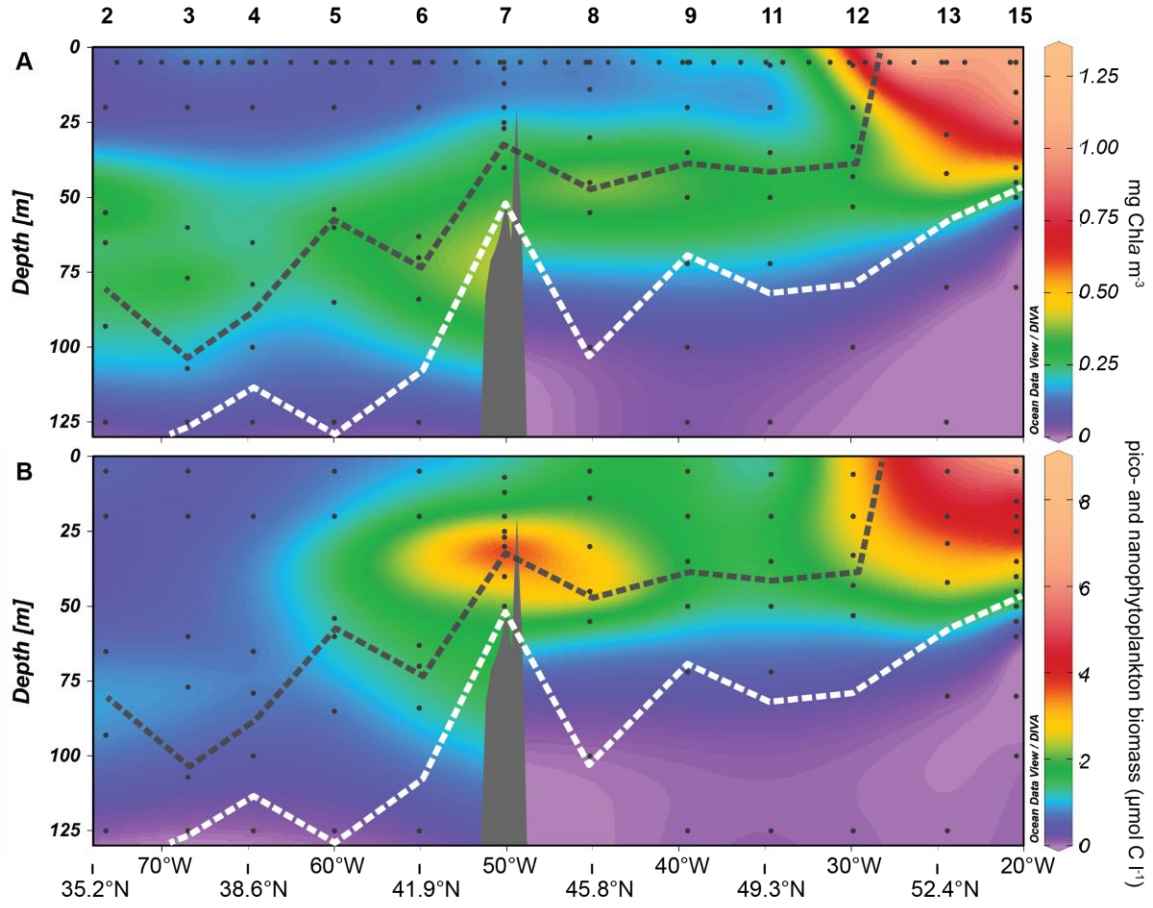

Figure 7. Depth-integrated chlorophyll *a* (ΣChla) in each size fraction (<2 µm, 2-20 µm and >20 µm) above the light compensation depth (Z_{lc}, see Table 1) as a percentage of the total integrated Chla measured at each station (solid black line).

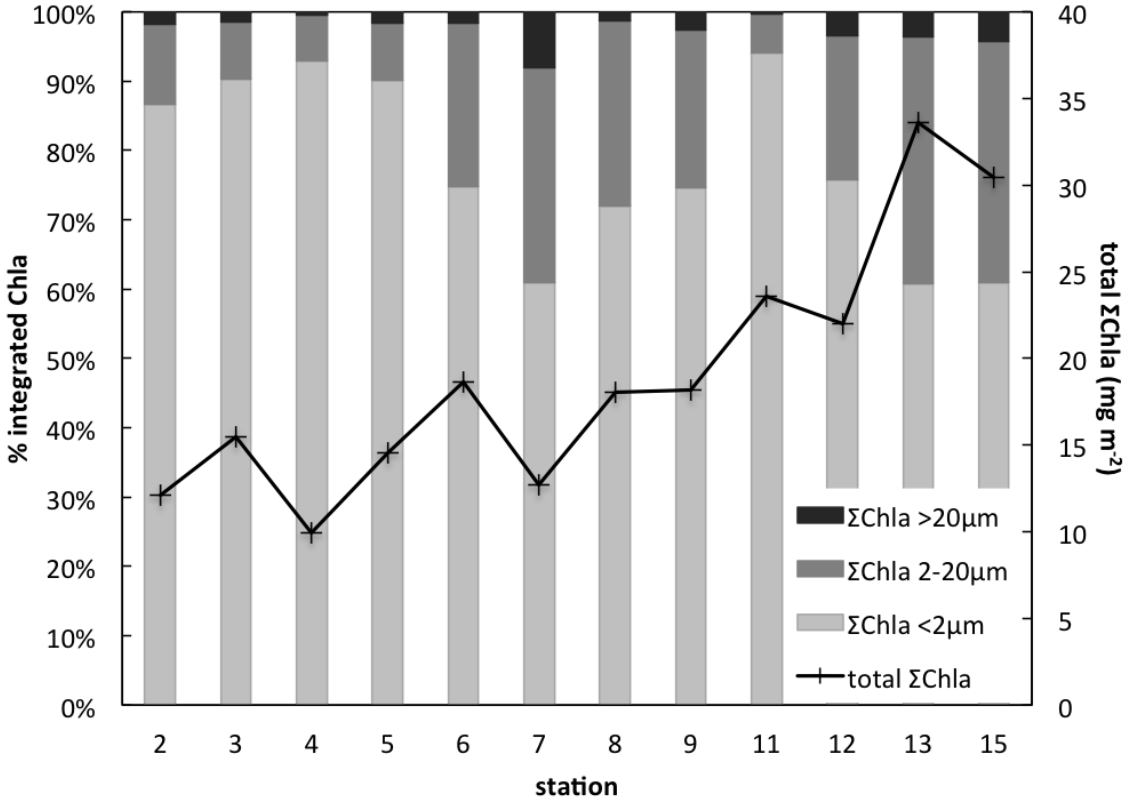

Figure 8. Depth section plots of the carbon biomass concentration of (A) *Prochlorococcus*, (B) *Synechococcus*, (C) picoeukaryotes, and (D) nanophytoplankton as enumerated by flow cytometry across the transect course. Dotted profile samples are associated with the station numbers listed at the top of the figure. The thick grey dashed line indicates the depth of the nitracline ($[NO_3^-]$ = 300 nmol l^{-1}). Note the

difference in colour bar scale for each phytoplankton group.

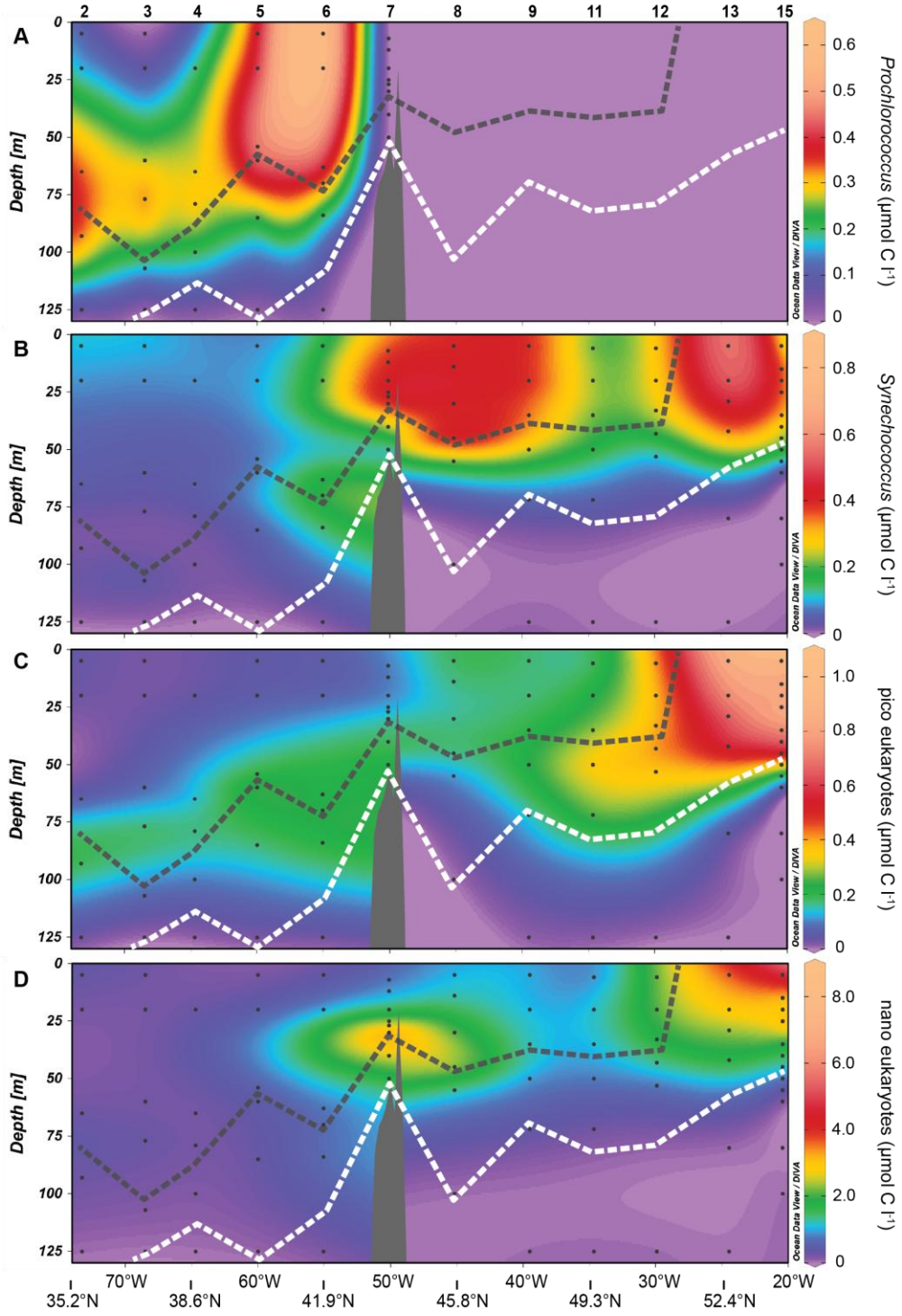

Figure 9. Depth section plots of the proportion of biomass represented by (A) *Prochlorococcus*, (B) *Synechococcus*, (C) picoeukaryotes, and (D) nanoeukaryotes as determined by flow cytometry. The thick grey dashed line indicates the depth of the

nitracline ([NO_3^-] = 300 nmol l^{-1}) and the thick white dashed line represents the light compensation depth (Z_{lc} at 0.17 mol PAR quanta m^{-2} day^{-1}). Dotted profile samples are associated with the station numbers listed at the top of the figure. Samples with a potentially unrepresentative population estimates (<250 nanophytoplankton cells counted) are greyed-out. Note that the different phytoplankton groups are plotted using different colour scales selected to emphasize their distribution patterns.

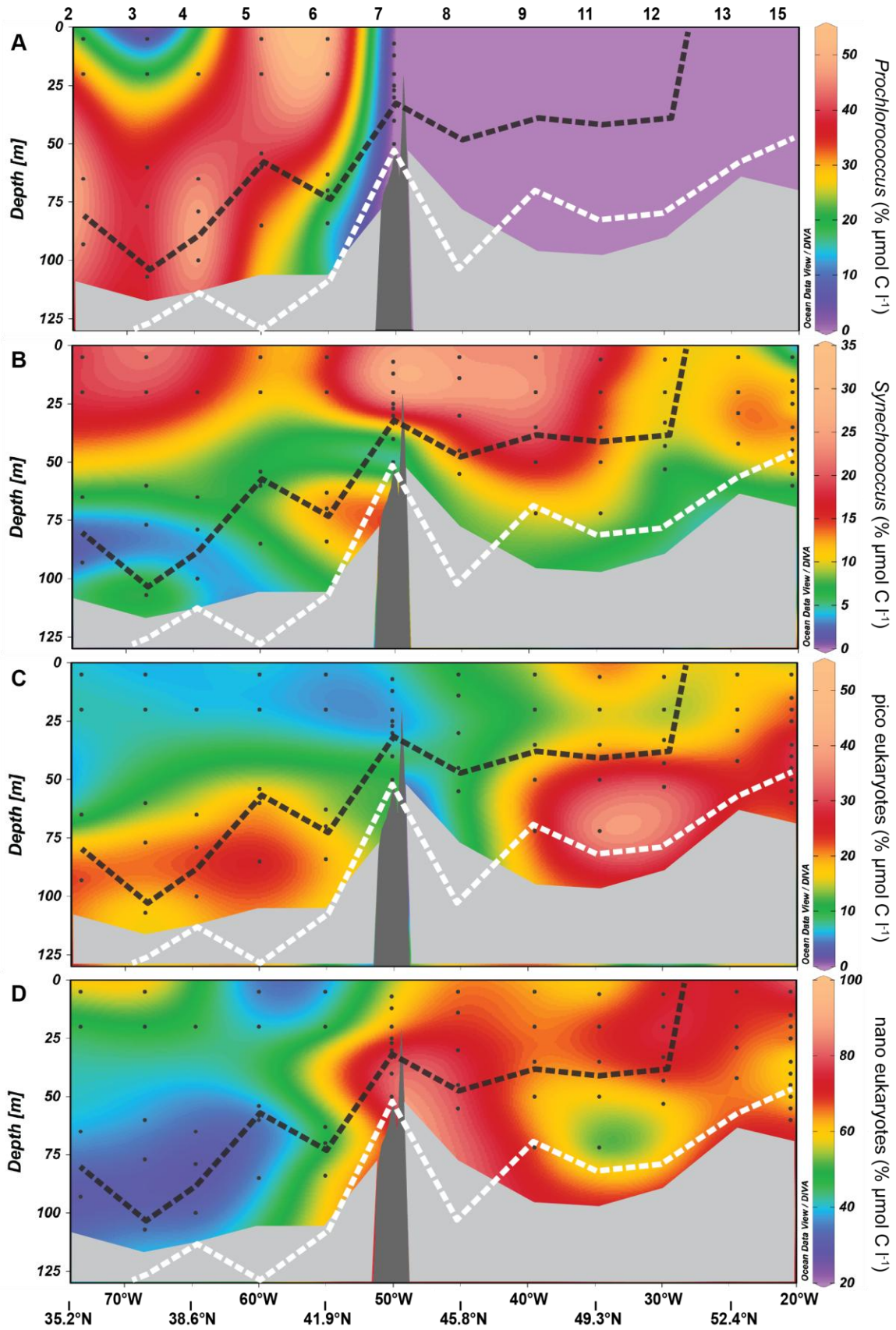
A
B
C
D
Depth [m]
0
25
50
75
100
125
2
3
4
5
6
7
8
9
11
12
13
15
70°W
60°W
50°W
40°W
30°W
20°W
35.2°N
38.6°N
41.9°N
45.8°N
49.3°N
52.4°N
Ocean Data View / DIVA
Prochlorococcus (% µmol C l-1)
Synechococcus (% µmol C l-1)
pico eukaryotes (% µmol C l-1)
nano eukaryotes (% µmol C l-1)

1.1 **Figure 10.** Depth section plots of (A) inorganic carbon fixation rate (transport rate; ρDIC) and (B) inorganic carbon fixation rate normalised to flow cytometry-derived phytoplankton biomass (specific rate; *V*DIC). The thick grey dashed line indicates the depth of the nitracline ([NO_3^-] = 300 nmol l^{-1}). Dotted profile samples are associated with the station numbers listed at the top of the figure.

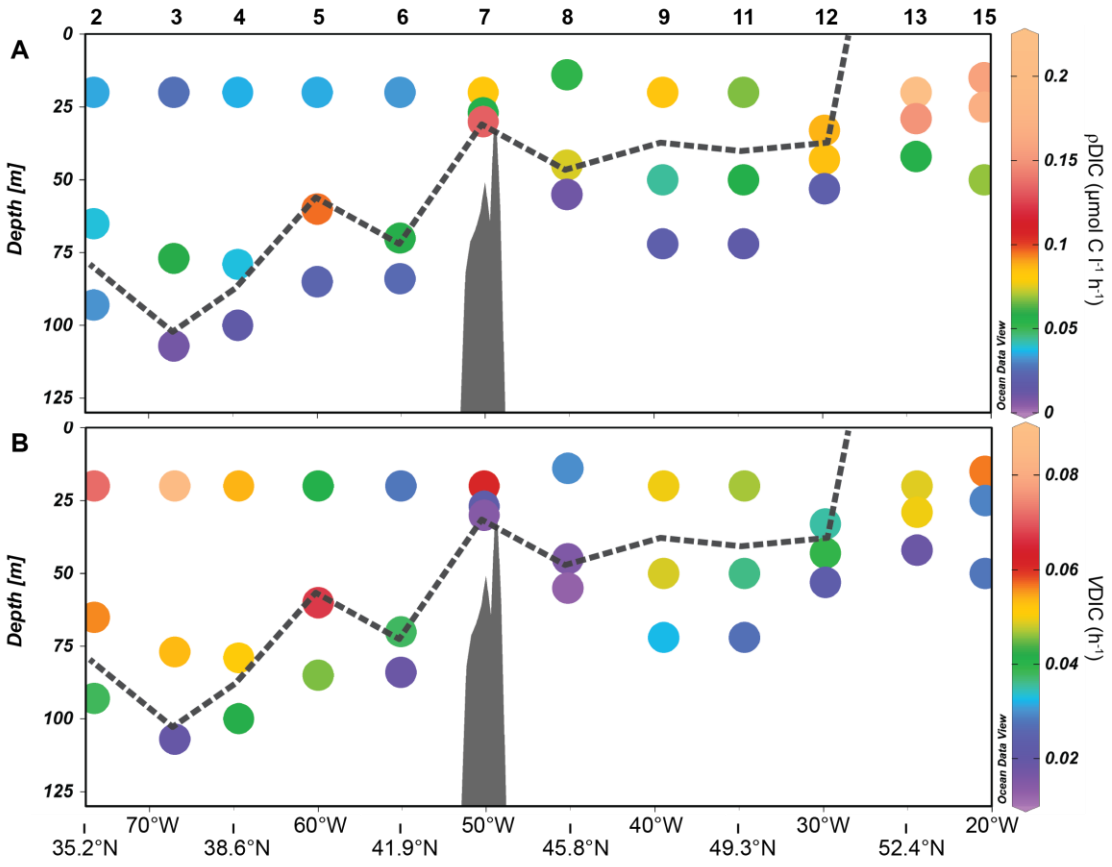

Table 1. Location and sampling date of transect stations. Z_{eu}: euphotic zone depth at 1% of surface PAR; MLD: mixed layer depth; Z_{lc}: light compensation depth; ΣChla: depth-integrated Chla from surface to Z_{lc}.

transect section	station	date	latitude (°N)	longitude (°W)	Z_{eu} (m)	Z_{lc} (m)	MLD (m)	nitracline depth (m)	300 nmol $[NO_3^-]$ l^{-1} isopleth (m)	ΣChla (mg m^{-2})
	2	2013-08-23	35.55	73.27	115	143	26	65	79	12.1
	3	2013-08-24	37.44	68.51	103	126	33	107	101	15.5
southwest	4	2013-08-25	38.78	64.71	120	115	45	79	85	9.9
	5	2013-08-26	40.27	60.00	106	130	30	54	57	14.6
	6	2013-08-27	41.90	55.06	90	108	21	70	71	18.7
shelf	7	2013-08-28	43.96	50.13	57*	57*	22	30	33	12.7
	8	2013-08-29	45.74	45.17	83	101	17	45	46	18.0
	9	2013-08-30	47.71	39.50	77	71	30	35	37	18.2
northeast	11	2013-08-31	49.35	34.69	71	82	28	35	41	23.5
	12	2013-09-01	50.93	29.90	70	79	38	33	37	22.0
	13	2013-09-02	52.64	24.45	50	58	36	42	0	33.6
	15	2013-09-03	54.02	20.44	52	47	39	45	0	30.4

*Because of the low value of the derived light attenuation coefficient at station 7, the bottom depth is listed instead of Z_{eu} and Z_{lc}.

Table 2. Planktonic groups quantified by flow cytometry and distinguished based on their fluorescence and light scattering properties. These properties included chlorophyll (Chla) fluorescence (fluo.), phycoerythrin (PE) fluo., light side scatter (SSC) and forward scatter (FSC) signals. Nanoeukaryote phytoplankton (nanoEuks) include noPE-, PE-nanoEuk and Cocco (see text for explanation of abbreviations).

planktonic group	group abbreviation	cell size (μm)	Chl fluo.	PE fluo.	SSC vs. FSC	stained DNA fluo.
non-PE nanoeukaryote phytoplankton	noPE-nanoEuk	~2.5 - 14	yes	no	low	-
PE nanoeukaryote phytoplankton	PE-nanoEuk	~2.5 - 14	yes	yes	low	-
coccolithophore	Cocco	~2.5 - 14	yes	no	high	-
picoeukaryote phytoplankton	picoEuk	~1 - 2.5	yes	no	low	-
Synechococcus	-	~1	yes	yes	low	-
Prochlorococcus	-	<1	yes	no	low	yes
heterotrophic bacteria	-	<1	no	no	low	yes

Table 3. Pearson correlation coefficient between different biogeochemical and/or physical variables measured in the upper 145 m of the water column. Heterotrophic bacterial cell abundance (het. bact. cell abund.), temperature (T), relative carbon biomass contribution of nanoeukaryote phytoplankton (%nanoEuk C) to total flowcytometric phytoplankton biomass (FCM phyto C), relative carbon biomass contribution of *Prochlorococcus* and *Synechococcus* to FCM phyto C (%picocyano C), upper ocean mass-weighted average $\delta^{15}N$ of suspended PN ($\delta^{15}N_{PN}$) minus the $\delta^{15}N$ of the subsurface nitrate source ($\delta^{15}N_{PN}$ - $\delta^{15}N_{NO3}$).

variable y	variable x	Pearson's *r*	*p*	n	data subset
nitracline depth	Z_{eu}	0.56	>0.05	12	upper 125 m
nitracline depth	Z_{lc}	0.64	<0.05	12	upper 145 m
nitracline depth	MLD	0.18	>0.05	12	upper 125 m
nitracline depth	$\delta^{15}N_{PN}$	-0.73	<0.01	11	above nitracline depth or MLD
nitracline depth	$\delta^{15}N_{PN}$ - $\delta^{15}N_{NO3}$	-0.53	>0.05	11	above nitracline depth or MLD
%nanoEuk C	$\delta^{15}N_{PN}$	0.91	<0.001	11	above nitracline depth or MLD
%nanoEuk C	$\delta^{15}N_{PN}$ - $\delta^{15}N_{NO3}$	0.75	<0.01	11	above nitracline depth or MLD
%picocyano C	$\delta^{15}N_{PN}$	-0.93	<0.001	11	above nitracline depth or MLD
%picocyano C	$\delta^{15}N_{PN}$ - $\delta^{15}N_{NO3}$	-0.84	<0.005	11	above nitracline depth or MLD
POC	PN	0.91	<0.001	33	55, 30 and 1% light depths
POC	FCM phyto C	0.91	<0.001	36	55, 30 and 1% light depths
POC	Chla	0.83	<0.001	34	55, 30 and 1% light depths
het. bact. cell abund.	FCM phyto C	0.85	<0.001	94	upper 125 m
het. bact. cell abund.	Chla	0.84	<0.001	81	upper 125 m
het. bact. cell abund.	ρDIC	0.76	<0.001	36	55, 30 and 1% light depths
ρDIC	POC	0.70	<0.001	36	55, 30 and 1% light depths
ρDIC	Chla	0.76	<0.001	34	55, 30 and 1% light depths
ρDIC	FCM phyto C	0.73	<0.001	36	55, 30 and 1% light depths
*V*DIC	T	0.70	<0.001	36	55, 30 and 1% light depths
*V*DIC	%nanoEuk C	-0.42	<0.05	36	55, 30 and 1% light depths
*V*DIC	%nanoEuk C	-0.46	<0.05	24	55 and 30% light depths
*V*DIC	%nanoEuk C	-0.80	<0.005	12	30% light depth

%nanoEuk C	T	-0.77	<0.001	36	55, 30 and 1% light depths
%nanoEuk C	T	-0.77	<0.001	24	55 and 30% light depths
%nanoEuk C	T	-0.89	<0.001	12	30% light depth